In vivo strains in the femur of the nine-banded armadillo (*Dasypus novemcinctus*)

by

Joseph V. Copploe II

Submitted in Partial Fulfillment of the Requirements

for the Degree of

Master of Science

in the

Biological Sciences

Program

YOUNGSTOWN STATE UNIVERSITY

May, 2014

In vivo strains in the femur of the nine-banded armadillo (*Dasypus novemcinctus*)

Joseph V. Copploe II

I hereby release this thesis to the public. I understand that this thesis will be made available from the OhioLINK ETD Center and the Maag Library Circulation Desk for public access. I also authorize the University or other individuals to make copies of this thesis as needed for scholarly research.

Signature:

Joseph V. Copploe II, Student Date

Approvals:

Dr. Michael T. Butcher, Thesis Advisor Date

Dr. Mark D. Womble, Committee Member Date

Dr. Thomas P. Diggins, Committee Member Date

Dr. Sal Sanders, Associate Dean, School of Graduate Studies Date

ABSTRACT

Understanding of the interplay between bone loading patterns and bone material properties in mammals has been based primarily on evidence from upright eutherians, which show limb bones that are loaded predominantly in anteroposterior (AP) bending with minimal torsion. However, loading patterns from the femora of marsupial opossums using crouched limb posture, show appreciable torsion while the bone experiences mediolateral (ML) bending. These data indicated greater locomotor loading diversity than was previously recognized, and suggested the possibility that ancestral loading patterns found in sprawling reptiles might have been retained among basal mammals. To further test this hypothesis, *in vivo* locomotor strains were recorded from the femur of the nine-banded armadillo (*Dasypus novemcinctus*). Orientations of principal strains and magnitudes of shear strains indicate that their femora are exposed to a limited amount of torsion, while loading is dominated by ML bending that places the medial aspect of the femur in compression and the lateral aspect in tension. This orientation of bending is similar to that found in opossums, but planar strain analyses indicate much more of the armadillo femur experiences tension during bending, potentially due to the actions of large muscles attached to the robust third trochanter (T3). Comparisons of peak locomotor loads to evaluations of femoral mechanical properties lead to estimates of limb bone safety factors between 2.3–5.0 in bending, similar to other eutherians, but lower than opossums and most sprawling taxa. Thus, femoral loading patterns in armadillos show a mixture of similarities to both opossums (ML bending) and eutherians (limited torsion and low safety factors), along with unique features (high axial tension) that likely relate to their distinctive hindlimb anatomy.

ACKNOWLEDGEMENTS

I sincerely thank my advisor, Dr. Michael Butcher, for all his guidance and mentoring throughout my Thesis research project and Masters Degree. I thank my graduate committee members, Drs. Mark D. Womble and Thomas P. Diggins for critical reviews of my Thesis and their helpful comments. I am extremely grateful to W. Loughry (Valdosta State University) for coordination and assistance with armadillo collection, Drs. Rick Blob (Clemson University) and John Parrish (Godley-Snell Research Center) for performing surgeries and data collection, and the entire staff at the GSRC for surgical assistance and animal care. Special thanks to J. DesJardins who provided access to mechanical testing equipment, and Roy Rusly (both at Clemson Bioengineering) assisted with mechanical property analyses. Thanks to Sue Klacik (St. Elizabeth Hospital, Youngstown, Ohio) for gauge sterilization. D. Lieberman (Harvard University) provided software for planar analysis of limb bone strains. The Georgia Department of Natural Resources (GDNR) coordinated permission for field collection of armadillos. Transport permits were coordinated by both GDNR and the South Carolina Department of natural Resources (SCDNR). This work was supported by STEM College funding (YSU) and Clemson Biological Sciences. The Youngstown State University and Clemson University Departments of Biological Sciences are also gratefully acknowledged.

DEDICATION

I dedicate this Thesis to my family, especially my mother Toni and my father Joe for their unfaltering support, both emotionally and financially, throughout my academic career and during the completion of this Thesis.

TABLE OF CONTENTS

Approval Page	ii
Copyright Page	iii
Abstract	iv
Acknowledgments	v
Dedication	vi
Table of Contents	vii
List of Tables	viii
List of Figures	ix
INTRODUCTION	1
MATERIALS and METHODS	3
Experimental animals	3
Surgical procedures and Gauge implantation	3
In vivo strain recordings and Data analysis	5
Mechanical properties and Safety factors	7
Statistics	7
RESULTS	8
Locomotor strain patterns and Magnitudes	8
Planar strain distribution and Neutral axis orientation	9
Bone mechanical properties and Safety factors	10
DISCUSSION	10
Loading patterns in the armadillo femur compared with other taxa	10
Comparison of in vivo loading data with mechanical models	12
Mechanical properties of the armadillo femur	12
Conclusions	14
REFERENCES	15
APPENDIX	24
Literature review	24

LIST OF TABLES

1. Morphometric data for all experimental animals 38

2. Peak axial (ε_{axial}), principal tensile (ε_t), principal compressive (ε_c), angle phi (ϕ_t), and shear strains recorded from the femur of *D. novemcinctus* 39

3. Mechanical properties, estimated actual peak strains and safety factors for the femur of *D. novemcinctus* loaded in three-point bending 40

LIST OF FIGURES

1. Anatomical drawing of the right hindlimb of *D. novemcinctus* 42

2. Representative strain recordings from three gauge locations on the femur of armadillo a04 during treadmill locomotion 44

3. Neutral axis orientation in the armadillo femur during treadmill locomotion 46

4. Graphical comparisons of cross-sectional planar strain analyses in the femur 48

5. Mechanical properties testing in bending for the armadillo femur 50

INTRODUCTION

During terrestrial locomotion, the limbs of vertebrate tetrapods can be exposed to loads that place substantial demands on the skeleton (Biewener, 1990, 1993). Much of the initial understanding of bone loading was derived from studies of cursorial, eutherian mammals that used upright, parasagittal limb kinematics (Rubin and Lanyon, 1982; Biewener et al., 1983, 1988). These taxa showed several common features in their loading patterns including: (1) loading regimes were dominated by anteroposterior (AP) bending with minimal indication of torsion (Rubin and Lanyon, 1982; Biewener et al., 1983, 1988; Biewener and Taylor, 1986), and (2) safety factors for limb bones typically ranged between 2 and 4 in their primary loading regime (Alexander, 1981; Biewener, 1983, 1993). However, more recent studies have shown that other tetrapod taxa diverge from these eutherian patterns (Blob et al., 2014). Many non-avian reptiles (e.g., lizards, alligators, and turtles) and amphibians (e.g., salamanders and frogs) use a sprawling limb posture in which the limbs move primarily in the transverse plane (Walker, 1971, 1973; Brinkman, 1981; Gatesy, 1991; Ashley-Ross, 1994; Marsh, 1994). Correlated with this locomotor posture, their limb bones are exposed to substantial torsional loads as well as moderate bending and have higher safety factors that range from 4.4–10.8 in bending (Blob and Biewener, 1999; Butcher et al., 2008; Sheffield et al., 2011; Blob et al., 2014). These comparatively elevated safety factors in non-avian reptiles and amphibians typically result from a combination of both lower bone loading magnitudes and higher material resistance to failure (Blob et al., 2014).

Although the distinctions in limb bone loading between sprawling taxa and cursorial eutherians were substantial, the patterns of loading observed were based on only a limited diversity of eutherians with generally similar limb kinematics and body plans. Recent data on femoral loading from Virginia opossums (Butcher et al., 2011; Gosnell et al., 2011) expanded perspectives on mammalian bone loading by sampling a species that (as a marsupial) was a phylogenetic out-group to other mammals in which bone loading had been evaluated, and that used a crouched limb posture during locomotion. Results from opossums showed several differences from eutherians and similarities to sprawling taxa. First, while bending was appreciable in the opossum femur, it was mediolateral (ML) in orientation rather than AP. Second, torsional loading was much higher than had been

observed in larger cursorial mammals and was similar in significance to values reported for rats (Keller and Spengler, 1989), small eutherians that also run with crouched limbs. Third, femoral safety factors in bending ranged from 5.1–7.2, generally intermediate between those of upright mammals and sprawling reptiles. These findings suggested that some of the distinctions in bone loading between eutherian and sprawling taxa might have evolved within the mammalian clade, rather than coincident with the origin of mammals (Blob et al., 2014). However, which loading traits might correspond with the use of crouched limb posture versus being eutherian remain unclear.

To address this issue and further refine understanding of the evolutionary history of limb bone loading patterns, *in vivo* strain and mechanical property data from the femur of nine-banded armadillos (*Dasypus novemcinctus*) have the potential to provide significant insights in these contexts. Armadillos use a crouched limb posture (Loughry and McDonough, 2013) and, as xenarthrans, belong to the most basal eutherian clade (Vizcaíno and Loughry, 2008; Delsuc et al., 2012). Therefore, retention of loading traits found in opossums would indicate features associated with crouched posture, rather than eutherian ancestry, while the loss of traits found in opossums might indicate features that emerged among eutherians in particular. In addition, armadillos possess unique osteological features that provide opportunities to evaluate the impact of structural novelties on bone loading, and to test predictions of proposed femoral loading models. Beyond their distinctive carapace composed of dermal scutes, armadillos (like other xenarthrans) have a robust third trochanter (T3) on the lateral aspect of the femoral shaft (McDonald and Iuliis, 2008; Milne et al., 2012) for the insertion of the *m. gluteus superficialis* and *m. tensor fasciae latae* (Milne and O'Higgins, 2012). Observing the T3 and the inherent medial curvature of the armadillo femur, recent finite element models of femoral loading in xenarthrans predicted that armadillo femora should experience ML bending during locomotion, placing the medial cortex of the femur in compression and the lateral cortex in tension (Milne and O'Higgins, 2012), Such loading patterns would match those observed in opossum femora (Butcher et al., 2011; Gosnell et al., 2011), but these models have yet to be validated by functional loading data.

The objective of this study was to record *in vivo* strains in the armadillo femur to further evaluate how bending, torsional loading, and safety factors changed throughout

mammalian evolution, and to test the extent of the correlation between these locomotor loading traits and the use of crouched limb posture. Based on modeling data (Milne and O'Higgins, 2012) and previous studies of opossums (Butcher et al., 2011; Gosnell et al., 2011), armadillo femora are predicted to be loaded in ML bending, with the lateral aspect exposed to tension and the medial to compression. Because armadillos locomote with crouched limbs and have attachments of major hip muscles on the T3 that may cause axial rotation of the femur (Milne and O'Higgins, 2012), they are also predicted to show appreciable femoral torsion similar to opossums (Butcher et al., 2011). Finally, with the expectations of loading magnitudes and regimes similar to those of opossums, limb bone safety factors of armadillos are predicted to match those of opossums. Discovery of such findings would support the conclusion that many loading features from cursorial eutherians are not general throughout the clade, and that some bone loading patterns from ancestral sprawling taxa may have been retained by mammalian species that locomote with crouched limbs.

MATERIALS AND METHODS

Experimental animals

Strain data were collected from N=3 armadillos, *Dasypus novemcinctus* (Linnaeus, 1758). Armadillos were trapped in Valdosta, GA using nets (animal collection permit: 29-WJH-13-166) and then transported to Clemson University (permit: S1-WJH-13-24). Animals were housed in medium-sized primate enclosures equipped with a pet carrier, provided with fresh water and litter pans, fed dog or cat food daily, and exposed to 12:12 hour light-dark cycles. Morphometric data for animals used in this study are presented in Table 1.

Surgical procedures and Gauge implantation

Strain gauges were attached surgically to the right femur of each animal using aseptic technique and following published methods (Biewener, 1992; Butcher et al., 2008, 2011). All surgical and experimental procedures were in accordance with protocols approved by the Clemson University IACUC (2013-030). Initial intramuscular doses of 2 mg kg^{-1} carprofen and 20 mg kg^{-1} ketamine were injected to induce analgesia and anesthesia, respectively, along with an intramuscular antibiotic injection (20 mg kg^{-1} Baytril).

Armadillos were then masked for general anesthesia (isoflurane), rested in lateral recumbency on a heating pad, and positioned to allow sterile surgical access to the medial aspect of the right hindlimb.

To expose strain gauge attachment sites, a longitudinal incision was made through the skin on the medial aspect of the thigh near mid-shaft, the location on long bones where strains are typically the highest (Biewener et al., 1986). Muscles surrounding the femur were separated along the fascial plane between the *m. vastus medialis* and *m. adductor magnus*, which were retracted to gain access to the femur. Strain gauges were attached at a level of the femur that approximated the distal-most portion of the T3. At the site where gauges were attached, a 'window' of periosteum was removed to expose the femoral cortex. Bone surfaces were scraped with a periosteal elevator, swabbed clean with ether using a cotton-tipped applicator, and allowed to dry for several seconds. Gauges were then attached using a self-catalyzing cyanoacrylate adhesive (Duro™ Superglue).

Single element (SE) and rosette (ROS) strain gauges (type FLG-1-11 and FRA-1-11, respectively; Tokyo Sokki Kenkyujo, Japan) were attached to three surfaces of the femur designated as 'anterior,' 'anteromedial,' and 'medial,' following absolute anatomical orientations for mammals. In one animal, it was possible to attach one gauge to the 'anterolateral' surface of the femur near the distal end of T3, and this gauge took the place of the 'anterior' implantation site used in the other animals (Fig. 1). Precise gauge locations were determined from dissection after the completion of the experiments. SE and the central elements of ROS were aligned (within 5 deg) to the long axis of the femur. With all three gauges in place, lead wires (336 FTE, etched Teflon; Measurements Group, Raleigh, NC, USA) were looped and sutured to muscle with 4-0 silk to provide strain relief, and then passed subcutaneously to the lateral aspect of the hip, where they were additionally passed through a hole drilled in the carapace. Once all incisions were sutured closed, lead wires were fitted through a Velcro® patch attached to the external surface of the carapace with epoxy resin, and then soldered into microconnectors. Solder connections were reinforced with epoxy to form a plug that was allowed to harden before being secured in the patch, thus providing security against mechanical damage to the lead wires before locomotor experiments.

In vivo strain recordings and Data analysis

After 1–2 days of recovery, *in vivo* strain recordings were collected from armadillos while the animals walked/ran on a motorized treadmill (model DC5; Jog A Dog®, Ottawa Lake, MI, USA). Strain signals were conducted from the gauges to Vishay conditioning bridge amplifiers (model 2120B; Measurements Group) via a shielded cable. Raw voltage signals from strain gauges were sampled through an A/D converter (model PCI-6031E; National Instruments Corp., Austin, TX, USA) at 5000 Hz, saved to computer using data acquisition software written in LabVIEW™ (v.6.1; National Instruments), and calibrated to microstrain ($\mu\varepsilon$ = strain $\times 10^{-6}$). Trials consisted of short bouts of steady-speed walking-running (belt speed: 0.12–0.55 m s^{-1}) with data sampled from 3–12 consecutive footfalls of the right hindlimb. In general, the speeds achieved by each armadillo required considerable exertion and were close to the maximal speed that the animals could sustain at a steady-state. Approximately two minutes of rest was given between each locomotor trial.

To document locomotor behavior and footfall patterns during experiments, a lateral view of strain trials was recorded with high-speed (100 Hz) video (Phantom V4.1; Vision Research Inc., Wayne, NJ, USA). Video data were synchronized with strain recordings using an LED visible in the video that simultaneously produced 1.5 V pulses visible in strain records. Upon completion of strain recordings, animals were anesthetized (isoflurane gas), and euthanized by an overdose of pentobarbital sodium solution (Euthasol®; 200 mg kg^{-1} intracardiac injection). Death was confirmed by inducing pneumothorax. Specimens were then dissected for verification of strain gauge placement, and frozen for later measurement of limb bone mechanical properties.

Standard conventions for analysis and interpretation of strain data were employed (Blob and Biewener, 1999; Butcher et al., 2008, 2011; Sheffield et al., 2011). Briefly, the magnitudes of peak axial strains (aligned with the long axis of the femur) were determined from each gauge location for n=30–60 steps from each armadillo (depending on available data). For each consecutive footfall, raw strains were zeroed at the time of foot contact with the tread (defined as “toe down”), with tensile strains recorded as positive and compressive strains as negative. The distribution of tensile and compressive strains on the femoral cortex then were used to evaluate the loading regime to which the

bone was exposed during locomotion. For instance, unequal magnitudes of tension and compression on opposite femoral cortices would indicate a combination of axial and bending loads. Magnitudes and orientations of peak principal strains (i.e., maximum and minimum strains at each site, regardless of alignment with the femoral long axis), as well as shear strain (i.e., torsional loading) magnitudes, were calculated from ROS data following published methods (Carter, 1978; Dally and Riley, 1978; Biewener and Dial, 1995). Defining the long axis of the femur as 0º, pure torsional loads would show principal strain orientations (deviations from the bone long axis) of 45º or -45º respectively, depending on whether the femur was rotated in a clockwise or counterclockwise direction.

Following dissections of the hindlimb musculature of each armadillo, instrumented femora were excised, swabbed clean of soft tissue, and embedded in fiberglass resin. Transverse sections were cut from two embedded femora through the mid-shaft gauge locations, and the cross-section of each bone was then photographed. The endosteal and periosteal outlines of the cross-sections from the photographs were traced in Adobe Illustrator, with the locations of the three gauges marked on the bone perimeter. The geometric data were then input along with peak strain data from the femoral gauge locations into analysis macros for the public domain software NIH Image for Macintosh, allowing calculation of the location of the neutral axis (NA) of bending and the planar distribution of longitudinal strains through femoral cross sections (Lieberman et al., 2003; Lieberman et al., 2004). Planar strain analyses were conducted on a subset of data (N=2 individuals; n=25 steps), in order to calculate estimates of peak tensile and compressive strain that may have occurred at locations other than recording sites (Carter et al., 1981; Biewener and Dial, 1995). For these analyses, the extreme projection of T3 was disregarded and the femur was modeled with an ovoid cross-section. Calculated peak strains were compared to measured peak strains to determine the proportional increase in strain between the recorded peaks and calculated peak magnitudes (Butcher et al., 2008, 2011). Additionally, in a subset of these data (n=18 steps), planar strain distributions and NA angle were calculated at five time points during a step (15%, 30%, 50%, 70% and 85% of contact) (Butcher et al., 2008, 2011) to evaluate shifts in the location and orientation of the NA throughout the step.

Mechanical properties and Safety factors

Mechanical properties in bending were measured as described for femora tested in previous studies (Butcher and Blob, 2008; Butcher et al., 2008; Wilson et al., 2009; Sheffield et al., 2011). Briefly, femora were extracted from thawed armadillo specimens, and muscle and periosteal tissue were cleaned away with moistened cotton swabs. Whole bones (N=4) were mounted in a three-point bending jig so the lateral aspect of the femur was loaded in tension. The anvils of the jig were positioned at a gauge length of 52 mm to provide stable seating for the bones between the anvils. SE gauges were glued to 'anterior,' 'anterolateral,' and 'posterior' surfaces of each bone near mid-shaft to record cortical strains during the bending tests. Gauge lead wires were soldered to a microconnector that was plugged into a shielded cable to convey raw strain signals to the Vishay amplifiers used during locomotor strain recordings. Amplified strain signals were sampled at 1000 Hz through an A/D converter in LabVIEW, and calibrated as detailed for *in vivo* recordings. Bones were loaded to failure in bending using a biaxial testing machine (Instron model 8874; Norwood, MA, USA: fitted with a 25 kN load cell) set with a cross-head displacement rate of 5 mm s^{-1} and applied load sampled at 100 Hz.

Yield points of the bones (reflecting failure) were identified from linear plots of applied bending moment (in Nm) versus maximum strain, based on the first point where measured strain magnitude deviated by 200 με from the magnitude expected based on the initial, linear slope of the curve (Currey, 1990). Planar strain analyses (as described above) were performed on strain magnitudes from all 3 gauges at the point of yield to calculate peak values of tensile and compressive strain during the bending tests (Wilson et al., 2009). Strain-based safety factors in bending for the femur of *D. novemcinctus* were calculated as the ratio of mean yield strains to mean peak strain magnitudes (recorded values corrected for proportional value of strain increase).

Statistics

Descriptive statistics of all data are reported as mean±s.d. (standard deviation) unless otherwise specified. Analysis of strain measurements (in με) was limited to the stance phase of the right hindlimb. Measured variables included axial strains (ε_{axial}) at each gauge location, principal tensile strains (ε_t), principal compressive strains (ε_c), angles of

off-axis loading (ϕ_t), and shear strains. Calculated variables included NA angle, calculated peak bending strains, yield bending strains, and bending safety factors.

RESULTS

Locomotor strain patterns and Magnitudes

The most frequent strain patterns in the femur of armadillos at a total of four different recording sites can be generalized as indicating that axial strains were tensile along the anterolateral-to-anterior aspect of the femur, and compressive on the anteromedial and medial surfaces of the femur (Fig. 2). Peak strain magnitudes were moderately variable among the three instrumented armadillos with coefficients of variation averaging 28.6% across SE recordings from the 'anteromedial' gauge location. Recorded strains for a01 at each location varied somewhat from those of a04 by showing overall higher tensile and compressive strains (Table 2). Patterns of tensile and compressive strains for all 3 individuals at the 'anteromedial' location were similar, but a01 experienced slightly different strain values recorded at the 'medial' location than the other two armadillos (Table 2). Despite these nuances in strain potentially related to absolute gauge location, the general similarities in strain patterns across individuals allowed us to evaluate characteristic loading magnitudes and regimes.

Axial strains at the 'anteromedial' location were consistently compressive throughout the step across individuals. For a03, axial strains recorded at that location were the highest among the three armadillos and averaged -682.8±290.6 με, while a04 had the lowest mean axial strains at this location with a value of -244.9±50.6 με. Strain patterns for a03 and a04 were different from those of a01, showing relatively low compressive strain magnitudes predominating at the 'medial' location, while a01 experienced nearly equal magnitudes of both compression and tension. Anterolateral strains were only recorded in a single individual (a01) and these were the highest absolute magnitudes of axial strain (tensile) recorded across the armadillos we tested (Table 2).

The timing of axial strain peaks was variable between individual armadillos. In a04, axial peaks from the 'anterior' location occurred slightly earlier than the axial strain peaks (and principal strain peaks) for the other two locations (Fig. 2). However, each of these peak strains occurred near mid-stance in all gauge locations at an average of

54.0±14.7% contact. In a01, peak strains occurred later in the step (71.5±11.4% contact) and were consistent across gauge locations. Principal strain recordings showed a single peak, with principal compressive strains very consistent across individuals irrespective of gauge location, averaging -779.0±216.9 με across individuals (Table 2). Peak principal tensile strains were lower than the principal compressive strains and were more variable among individual armadillos.

Principal and shear strains also indicate that armadillo femora experience some torsion. Average orientations of peak principal tensile strain (ϕ_t) on the 'anteromedial' and 'anterior' surface of the femora of a03 and a04 showed minor deviations from the long axis of the bone (Fig. 2), averaging 15.5±6.4º across individuals (Table 2) that indicated medial rotation of the femur during the step. However, these values are far from an angle of 45º expected for pure torsional loading and peak shear strains were generally low, averaging 261.8±179.0 με across individuals, or 66% lower than peak compressive principal strains (Table 2; Fig. 2).

Planar strain distribution and Neutral axis orientation

Planar strain analyses showed a consistent neutral axis (NA) orientation throughout the stance phase and indicated mediolateral (ML) bending in both individuals analyzed (a01 and a04: Figs. 3, 4). Gauge placement at the 'anterolateral' location on the femur in a01 allowed the only direct record of high tensile strains laterally, and helped to facilitate more confident estimates of peak strains via planar strain analysis by accounting for a larger portion of the femoral cross-section. Though some variation in absolute NA orientation and location about the femur cross-section was evident (Fig. 4), similar patterns emerged across the trials analyzed, particularly through the first half of the step (i.e., the first three time points evaluated).

At the beginning of the step, the NA was typically aligned close to the anatomical AP axis and tended to shift far medially from the cross-sectional centroid early in the step (Figs. 3, 4), placing the lateral cortex under high tensile loading. As strain magnitudes increased through the step (30–70% contact), the NA maintained this orientation, changing only a few degrees, but became slightly less aligned with the anatomical AP axis for a01 (Figs. 3, 4). This trend was also evident for individual a04, except the NA became more closely aligned with the anatomical AP axis through the entire step and

peak strains occurred at 50% contact (Fig. 4). The medial displacement of the NA from the centroid and the extent of tensile strains across the femoral cross-section confirm loading in ML bending for armadillo femora, as previously observed in opossums (Butcher et al., 2011; Gosnell et al., 2011).

Planar strain data indicate that peak tensile strains occur on the lateral aspect of the femur in armadillos, and peak compressive strains on the medial surface. Calculated peak strains on the medial aspect of the femur were higher than the peak strains at the precise locations from which strains were recorded in the test animals. Based on the distribution of planar strain contours (Fig. 4), actual peak compressive strains in the armadillo femur are likely similar to those recorded, averaging just 1.04±0.10 higher, but ranged between 1.0–1.42 across trials in which planar strain distributions were calculated (n=31 steps). Actual peak tensile strains in the armadillo femur appear to be much higher than those recorded with a proportional increase in strain averaging 3.99±0.63.

Bone mechanical properties and Safety factors

Each bone failed catastrophically in bending, with yield and fracture occurring nearly simultaneously (Fig. 5A). Planar strain analysis of the bending tests resulted in average yield strains of 3716.7±419.1 με in tension and -4168.4±2802.6 με in compression (Table 3; Fig. 5B) for armadillo femora. Prior to calculating safety factors, peak recorded functional strains during locomotor trials were multiplied by either 3.99 (tensile) or 1.04 (compressive) to reflect the predicted proportional increases in strain (Table 3). Based on the highest strains (principal) determined across individuals, mean values of 1614.2 με and -831.3 με were calculated and used to generate limb bone safety factors. The ratio of the bending yield strain to peak functional strain produced safety factor estimates of 2.3 in tension and 5.0 in compression (Table 3).

DISCUSSION

Loading patterns in the armadillo femur compared with other taxa

In vivo strain recordings indicated the armadillo femur is exposed to substantial ML bending with a limited amount of torsion. Planar strain analyses showed that bending placed a large portion of the lateral femoral cortex under tensile loading, whereas a smaller portion of the medial cortex experienced compression (Fig. 4). Because

armadillos and Virginia opossums are similar in their size, cursorial tendencies, and use of crouched limb posture, we expected close correspondence between the loading patterns of these two representative basal mammals. However, the loading magnitudes and regimes we recorded from nine-banded armadillos only partially match this prediction.

Peak shear strains from armadillo femora were less than half the value of shear strains in the opossum femur (Butcher et al., 2011), and close to the magnitudes found in the distal limb bones of upright running animals (Main and Biewener, 2007). In contrast, rats have been shown to experience high torsion in their femur (Keller and Spengler, 1989) and are the only eutherian mammals using crouched limb posture for which high torsional loading has been observed. Unfortunately, detailed kinematic comparisons across these species that might help to explain such differences are not available. Another deviation of armadillos from loading patterns in opossums and rats, was the low ϕ_t angle found in armadillos, which was similar to that in upright mammals (Biewener et al., 1983, 1988; Main and Biewener, 2004). Both armadillos used for planar strain analysis also showed very little change in NA orientation through the step similar to findings from dogs, horses, and goats, where the angle of principal strain changed by only a few degrees during limb stance (Rubin and Lanyon, 1982; Biewener and Taylor, 1986). This finding indicates that the orientation of bending was maintained while the limb was supporting the load of the animal. In particular, the pronounced mediolateral curvature of the armadillo femur (Milne and O'Higgins, 2012) may constrain loading to predominantly, and predictably, bend the femur in that direction (Bertram and Biewener, 1988; Jade et al., 2014).

Mean principal compressive strains in the armadillo were similar in magnitude to those recorded in the femora of non-avian reptiles (Blob and Biewener, 1999; Butcher et al., 2008) and rats (Keller and Spengler, 1989), but were lower than the typical principal strains recorded in upright mammals (Biewener and Taylor, 1986). Although mean principal compressive strains greatly exceeded the magnitudes of mean principal tensile strains at our recording sites, principal strains were not recorded from the 'anterolateral' location on the femur, which had the highest recorded magnitudes of axial tensile strain. A ROS gauge could not be implanted on this femoral surface in the experimental animals

due to the T3 and large investment of muscles along the lateral aspect of the hindlimb, and therefore, evaluations of peak tensile strains must be approached with some caution. Nonetheless, axial tensile strains on the femur were higher in armadillos than the axial strains experienced by the opossum femur (Butcher et al., 2011). It is possible that the extensive musculature invested on the lateral aspect of the femur by insertion on the T3 influences such loads by contraction during the step. A synchronization of bone strain recordings with fascicle strain and EMG recordings from these muscles could help evaluate this possibility (Aiello et al., 2013).

Comparison of *in vivo* loading data with mechanical models

In vivo loading data from *D. novemcinctus* show good general correspondence with the results of a published finite element model of loading in the femur of *Dasypus hybridus* (Milne and O'Higgins, 2012), a species of armadillo approximately half the body mass and body length of the animal that was the focus of this study. Applying a 60 N force as a load parameter produced an expectation of mediolateral bending, with magnitudes of peak compressive strains of -250 to -500 με modeled for the medial cortex (Milne and O'Higgins, 2012). *In vivo* data verified this predicted orientation of ML bending, and recorded axial strains in *D. novemcinctus* were typically within the predicted range, although recorded principal compressive strains did exceed -700 με (Table 2). Peak recorded tensile strains showed less correspondence with the model results, again potentially reflecting an influence of T3 that is difficult to predict.

Mechanical properties and Safety factor of the armadillo femur

Bending yield strains in the armadillo femora were low compared to available yield strain data found in other vertebrate taxa (Biewener, 1982, 1993; Erickson et al. 2002; Butcher et al., 2008, 2011). Mean yield strain values for the armadillo femur in tension (3716.7 με) and compression (-4168.4 με) fell well below the range of values reported for the femur [6700–9300 με (Erickson et al., 2002)] in numerous species of amphibians, non-avian reptiles, and basal mammals (e.g., Monotremata, Marsupalis, and Eutheria). In the study by Erickson et al. (2002), yield strains from three-point bending tests on whole femora were calculated as the quotient of bending strength and Young's modulus as opposed to strains being measured directly by attached strain gauges in this study. This

may explain some differences in tensile yield strains obtained between studies; however, using similar methods as our study, much higher yield strains were previously reported for the limb bones of non-avian reptiles (Butcher et al., 2008; Sheffield et al., 2011; Blob et al., 2014), amphibians (Wilson et al., 2009), and opossums (Butcher et al., 2011). On average, these taxa were found to have higher yield strains than the values typical for the limb bones of upright mammals and birds [6000–8000 με (Currey, 1984)]. The crosshead speed in the present experiments was faster (5 mm s^{-1} vs. 5 mm min^{-1}) than in previous studies, and while loading rates can influence mechanical properties, bones loaded at high rates can typically withstand higher, rather than lower, strains before yield failure (Currey, 1988; Courtney et al., 1994; Yeni and Fyhrie, 2003; Földhazy et al., 2005). Although *D. novemcinctus* appear to have yield strains less than the range typical for upright mammals, there are no other limb bone data from xenarthrans available for comparison, so it is unclear whether this property reflects generally lower failure resistance in xenarthran limb bones.

The low yield strains in armadillo femora are surprising given that they are eutherian mammals, and both material and mechanical properties are usually expected to be conserved across related taxa (Currey, 2002; Erickson et al., 2002). One physiological factor that might help explain the low resistance to failure in armadillo limb bones is their investment of dermal bone in the body armor (carapace and tail), which may require selective resorption of calcium and minerals from the limb bones. Evaluations of bone mineral content could address this possibility, but in this context it bears noting that turtles, which also invest bone in dermal armor, do not show reductions of material strength in their limb bones (Butcher and Blob, 2008; Butcher et al., 2008).

Safety factors were calculated based on recordings of peak *in vivo* locomotor strains and bone mechanical properties. Given the prominence of bending over torsion as an *in vivo* loading regime, these evaluations focused only on bending. Estimates for safety factors in bending were calculated from both tensile and compressive strains and were lower than those predicted based on expected similarities to opossums. Values of 2.3–5.0 for armadillo limb bone safety factors in bending are more typical of those in the ranges found among upright mammals (Alexander, 1981; Lanyon and Rubin, 1985; Biewener, 1993; Blob et al., 2014). Safety factors for armadillo femora at best approach the low end

values for the opossum [5.1–7.2 (Butcher et al., 2011)], and were low compared with strain-based safety factors estimated for several species of non-avian reptiles in previous studies [range: 6.3–10.8 (Blob and Biewener, 1999; Butcher et al., 2008; Sheffield et al., 2011)]. Low yield strains appear to be a primary factor leading to the low safety factors for the armadillo femur, with levels of peak functional strain less of a contributing factor. If low yield strains (and safety factors) are characteristic of xenarthran limb bones, then some apparent similarities in bone design between upright mammals and armadillos still may have emerged through independent evolutionary paths, because their safety factors may be achieved via different underlying causes.

Conclusions

The loading patterns of the armadillo femur show similarities to mammals from basal lineages like opossums (e.g., mediolateral bending), and derived cursorial eutherians (e.g., reduced torsion and lower safety factors). However, it is not appropriate to regard armadillos as intermediate in their locomotor mechanics between crouched marsupials and upright eutherians. It is unclear when the reduction in limb bone torsion characteristic of cursorial eutherians may have evolved. This is because even though armadillos (as the most basal eutherians) show low torsional loading, rats (more closely related to cursorial eutherians) do not (Keller and Spengler, 1989). Moreover, although limb bone safety factors of armadillos may come closer to those of other eutherians than to those of marsupial opossums, such safety factors appear to be achieved through a predominantly different mechanism. The loading mechanics of armadillo femora are likely influenced by distinctive features of the family, including the robust T3, insertion of muscles on both the T3 and femoral shaft, and potential investment of mineral resources into a bony carapace. Without evaluations from species exhibiting similar distinctive anatomical characteristics and critical phylogenetic positions, it will be difficult to reveal the evolutionary history of mammalian locomotor loading mechanics. Future examinations of phylogenetically and functionally diverse taxa will continue to expand understanding of vertebrate locomotor diversity and its evolutionary origins (Blob et al., 2014).

REFERENCES

Aiello, B. R., Blob, R. W. and Butcher, M. T. (2013). Correlation of bone loading and muscle contractile function in the hindlimb of the river cooter turtle (*Pseudemys concinna*). *J. Morphol.* **274,** 1060–1069.

Alexander, R. M. (1981). Factors of safety in the structure of animals. *Sci. Prog*. **67,** 109–130.

Ashley-Ross, M. A. (1994). Hindlimb kinematics during terrestrial locomotion in a salamander (*Dicamptodon tenebrosus*). *J. Exp. Biol.* **193,** 255-283.

Ancona, K. A. and Loughry, W. J. (2009). Time budgets of wild nine-banded armadillos. *Southeast Nat.* **8,** 587–598.

Argot, C. (2002). Functional-adaptive anatomy of the hindlimb in the Didelphidae, and the paleobiology of the Paleocene marsupials *Mayulestes ferox* and *Pucadelphys andinus*. *J. Morphol.* **253,** 76–108.

Bertram, J. E. and Biewener, A. A. (1988). Bone curvature: sacrificing strength for load predictability? *J. Theor. Biol.* **131,** 75–92.

Biewener, A. A. (1982). Bone strength in small mammals and bipedal birds: do safety factors change with body size? *J. Exp. Biol.* **98,** 289–301.

Biewener, A. A. (1983a). Locomotory stresses in the limb bones of two small mammals: the ground squirrel and chipmunk. *J. Exp. Biol.* **103,** 131–154.

Biewener, A. A. (1983b). Allometry of quadrupedal locomotion: the scaling of duty factor, bone curvature and limb orientation to body size. *J. Exp. Biol.* **105,** 147–171.

Biewener, A. A. (1989). Scaling body support in mammals: limb posture and muscle mechanics. *Science* **245**, 45–48.

Biewener, A. A. (1990). Biomechanics of mammalian terrestrial locomotion. *Science* **250,** 1097–1103.

Biewener, A. A. (1992). *In vivo* measurement of bone strain and tendon force. In *Biomechanics – Structures and Systems: A Practical Approach* (ed. A. A. Biewener), p. 123–147. New York: Oxford University Press.

Biewener, A. A. (1993). Safety factors in bone strength. *Calcif. Tissue Int. (Suppl. 1).* **53,** S68–S74.

Biewener, A. A. and Bertram, J. E. A. (1993). Skeletal strain patterns in relation to exercise training during growth. *J. Exp. Biol.* **185,** 51–69.

Biewener, A. A. and Dial, K. P. (1995). *In vivo* strain in the humerus of pigeons (*Columba livia*) during flight. *J. Morphol*. **225,** 61–75.

Biewener, A. A. and Taylor, C. R. (1986). Bone strain: a determinant of gait and speed? *J. Exp. Biol.* **123,** 383–400.

Biewener, A. A., Thomason, J. J. and Lanyon, L. E. (1988). Mechanics of locomotion and jumping in the horse (*Equus*): *in vivo* stress in the tibia and metatarsus. *J. Zool., Lond.* **214,** 547–565.

Biewener, A. A., Thomason, J. J., Goodship, A. and Lanyon, L. E. (1983). Bone stress in the horse forelimb during locomotion at different gaits: a comparison of two experimental methods. *J. Biomech*. **16,** 565–576.

Biknevicius, A. R. (1999). Body mass estimation in armoured mammals: cautions and encouragements for the use of parameters from the appendicular skeleton. *J. Zool., Lond.* **248,** 179–187.

Blob, R. W. and Biewener, A. A. (1999). *In vivo* locomotor strain in the hindlimb bones of *Alligator mississippiensis* and *Iguana iguana*: implications for the evolution of limb bone safety factor and non-sprawling limb posture. *J. Exp. Biol.* **202,** 1023–1046.

Blob, R. W. and Biewener, A. A. (2001). Mechanics of limb bone loading during terrestrial locomotion in the green iguana (*Iguana iguana*) and American alligator (*Alligator mississippiensis*). *J. Exp. Biol.* **204,** 1099–1122.

Blob, R. W., Espinoza, N. R., Butcher, M. T., Lee, A. H., D'Amico, A. R., Baig, F., and Sheffield, K. M. (2014). Diversity of limb bone safety factors for locomotion in terrestrial vertebrates: evolution and mixed chains. *Integr. Comp. Biol.,* In press.

Breece, G. A. and Causey, M. K. (1973). Armadillo depredation of "dummy" bobwhite quail nests in southwest Alabama. *Proceeding of the Annual Conference of Southeastern Fish and Wildlife Agencies.* **27,** 18–22.

Brinkman, D. (1981). The hind limb step cycle of *Iguana* and primitive reptiles. *J. Zool., Lond.* **181,** 91–103.

Burr, D. B., Milgrom, C., Fyhrie, D., Forwood, M., Nyska, M., Finestone, A., Hoshaw, S., Saiag, E. and Simkin, A. (1996). In vivo measurement of human tibial strains during vigorous activity. *Bone.* **18,** 405–410.

Bushnell, R. (1952). The place of the armadillo in Florida wildlife communities. Master's Thesis, Stetson University, DeLand, Florida.

Butcher, M. T. and Blob, R. W. (2008). Mechanics of limb bone loading during terrestrial locomotion in river cooter turtles (*Pseudemys concinna*). *J. Exp. Biol.* **211,** 1187–1202.

Butcher, M. T., Espinoza, N. R., Cirilo, S. R. and Blob, R. W. (2008). *In vivo* strains in the femur of river cooter turtles (*Pseudemys concinna*) during terrestrial locomotion: tests of force-platform models of loading mechanics. *J. Exp. Biol*. **211,** 2397–2407.

Butcher, M. T., White, B. J., Hudzik, N. B., Gosnell, W. C., Parrish, J. H. A. and Blob, R. W. (2011). *In vivo* strains in the femur of the Virginia opossum (*Didelphis virginiana*) during terrestrial locomotion: testing hypotheses of evolutionary shifts in mammalian bone loading and design. *J. Exp. Biol.* **214,** 2631–2640.

Carrano, M. T. (1998). Locomotion of non-avian dinosaurs: integrating data from hindlimb kinematics, *in vivo* strains and bone morphology. *Paleobiol*. **24,** 450–469.

Carrano, M. T. and Biewener, A. A. (1999). Experimental alteration of limb posture in the chicken (*Gallus gallus*) and its bearing on the use of birds as analogs for dinosaur locomotion. *J. Morphol.* **240,** 237–249.

Carter, D. R. (1978). Anisotropic analysis of strain rosette information from cortical bone. *J. Biomech.* **11,** 199–202.

Carter, D. R., Harris, W. H., Vasu, R. and Caler, W. E. (1981). The mechanical and biological response of cortical bone to *in vivo* strain histories. In *Mechanical Properties of Bone* (AMD vol. 45) (ed. S. C. Cowin), p. 81–92. New York: American Society of Mechanical Energy.

Chen, I. H., Kiang, J. H., Correa, V., Lopez, M. I., Chen, P.-Y., McKittrick, J. and Meyers, M. A. (2011). Armadillo armor: Mechanical testing and micro-structural evaluation, *J. Mech. Behav. Biomed.* **4,** 713–722.

Clarke, A., Rothery, P. and Isaac, N. J. B. (2010). Scaling of basal metabolic rate with body mass and temperature in mammals. *J. Anim. Ecol.* **79,** 610–619.

Courtney, A. C., Wachtel, E. F., Myers, E. R. and Hayes, W. C. (1994). Effects of loading rate on strength of the proximal femur. *Calcif. Tissue Int.* **55,** 53-58.

Currey, J. D. (1970). The mechanical properties of bone. *Clin. Orthop. Relat. Res.* **73,** 210–231.

Currey, J. D. (1984) The mechanical adaptations of bone, Princeton University Press, Princeton.

Currey, J. D. (1988). The effect of porosity and mineral content on the Young's modulus of elasticity of compact bone. *J. Biomech.* **21,** 131-139.

Currey, J. D. (1990). Physical characteristics affecting the tensile failure properties of compact bone. *J. Biomech*. **23,** 837–844.

Currey, J. D. (2002). *Bones. Structure And Mechanics*. Princeton, NJ: Princeton University Press.

Dally, J. W. and Riley, W. F. (1978). *Experimental Strain Analysis*. New York: McGraw-Hill.

Davies, H. M., McCarthy, R. N. and Jeffcott, L. B. (1993). Surface strain on the dorsal metacapus of thoroughbreds at different speeds and gaits. *Acta Anat. (Basel).* **146,** 148–153.

Delsuc, F. and Douzery E. J. P. (2008). Recent advances and future prospects in xenarthran molecular phylogenetics. In *The Biology of the Xenarthra* edited by S.F. Vizcaíno & W.J. Loughry. Gainesville, FL: University Press of Florida, p. 11–23.

Delsuc, F., Superina, M., Tilak, M.-K., Douzer, E.J.P. and Hassanin, A. (2012). Molecular phylogenetics unveils the ancient evolutionary origins of the enigmatic fairy armadillos. *Mol. Phylogenet. Evol.* **62,** 673–680.

Denson, R. D. (1979). Aggression and tumbling among armadillos. *Southwest. Nat.* **24,** 697-698.

Erickson, G. M., Catanese, J. III. and Keaveny, T. M. (2002). Evolution of the biomechanical material properties of the femur. *Anat. Rec.* **268,** 115–124.

Fariña, R. A. and Vizcaíno, S. F. (1997). Allometry of the bones of living and extinct armadillos (Xenarthra, Dasypoda). *Z. Saugetierkunde*, **62,** 65–70.

Földhazy, Z., Arndt, A., Milgrom, C., Finestone, A. and Ekenman, I. (2005). Exercise-induced strain and strain rate in the distal radius. *J. Bone Joint Surg.* **87B,** 261-266.

Furman, B. R. and Saha, S. (2000). Torsional testing of bone. In *Mechanical Testing of Bone and the Bone-Implant Interface* (ed. Y. H. An. and R. A. Draughn), p. 219–239. Boca Raton: CRC press.

Gao, K. and Shubin, N. H. (2001). Late Jurassic salamanders from northern China. *Nature* **410,** 574–577.

Gatesy, S. M. (1991). Hind limb movements of the American alligator (*Alligator mississippiensis*) and postural grades. *J. Zool., Lond.* **224,** 577–588.

Gaudin, T. J. and Biewener, A. A. (1992). The functional morphology of xenarthrous vertebrae in the armadillo Dasypus novemcinctus (Mammalia, Xenarthra). *J. Morphol.* **214,** 63–81.

Gosnell, W. C., Butcher, M. T., Maie, T. and Blob, R. W. (2011). Femoral loading mechanics in the Virginia opossum, *Didelphis virginiana*: torsion and mediolateral bending in mammalian locomotion. *J. Exp. Biol.* **214**, 3455–3466.

Gross. T. S., McLeod, K. J. and Rubin, C. T. (1992). Characterizing bone strain distributions *in vivo* using three rosette strain gauges. *J. Biomech*. **25,** 1081–1087.

Hildebrand, M. (1960). How animals run. *Sci. Amer.* **5,** 148–157.

Hildebrand, M. (1985). Walking and Running. In: Hildebrand M, Bramble DM, Liem KF, Wake DB, editors. Functional Vertebrate Morphology. Cambridge, Massachusetts: The Belknap Press of Harvard University Press. p. 38–57.

Jade, S., **Tamvada, K. H., Strait, D. S. and Grosse, I.R.** (2014). Finite element analysis of a femur to deconstruct the paradox of bone curvature. *J. Theor. Biol.* **341,** 53-63.

Jenkins, F. A., Jr (1971). Limb posture and locomotion in the Virginia opossum (*Didelphis marsupialis*) and in other non-cursorial mammals. *J. Zool. Lond.* **165,** 303–315.

Kalmbach, E. R. (1943). *The Armadillo: Its Relation to Agriculture and Game.* Austin, Texas: U. S. Fish and Wildlife Service.

Keller, T. S. and Spengler, D. M. (1989). Regulation of bone stress and strain in the immature and mature rat femur. *J. Biomech.* **22,** 1115–1127.

Lanyon, L. E. and Bourn, S. (1979). The influence of mechanical function on the development and remodeling of the tibia. An experimental study in sheep. *J. Bone Jt. Surg*. **61A,** 263–273.

Lanyon, L. E. and Rubin, C. T. (1985). Functional adaptation in skeletal structures. In: Functional Vertebrate Morphology (ed. M. Hildebrand, D. M. Bramble, K. F. Liem and D. B. Wake), Cambridge: The Belknap Press. p. 1-25.

Lieberman, D. E., Pearson, O. M., Polk, J. D., Demes, B. and Crompton, A. W. (2003). Optimization of bone growth and remodeling in response to loading in tapered mammalian limbs. *J. Exp. Biol*. **206,** 3125–3138.

Lieberman, D. E., Polk, J. D. and Demes, B. (2004). Predicting long bone loading from cross-sectional geometry. *Am. J. Phys. Anthropol.* **123,** 156–171.

Loughry, W. J. and McDonough, C. M. (2013). *The Nine-Banded Armadillo: A Natural History (Animal Natural History Series).* Norman, OK: University of Oklahoma Press.

Main, R. P. and Biewener, A. A. (2004). Ontogenetic patterns of limb loading, *in vivo* strains and growth in the goat radius. *J. Exp. Biol.* **207,** 2577–2588.

Main, R. P. and Biewener, A. A. (2007). Skeletal strain patterns and growth in the emu hindlimb during ontogeny. *J. Exp. Biol.* **210,** 2676–2690.

Marsh, R. L. (1994). Jumping ability of anuran amphibians. *Adv. Vet. Sci. Comp. Med*. **38B,** 51–111.

McBee, K. and Baker, R. J. (1982). *Dasypus novemcinctus*. *Mammal. Spec.* **162,** 1–9.

McDonald, H. G. and De Iuliis, G. (2008). Fossil history of sloths. In: Vizcaíno SF, Loughry WJ (eds) Biology of the Xenarthra. University of Florida Press, Gainesville, Florida. p. 24–36.

McDonough, C. M. (1994). Determinants of aggression in nine-banded armadillos. *J. Mammal.* **75,** 189–198.

McDonough, C. M. and Loughry, W. J. (1995). Influences on vigilance in nine-banded armadillos. *Ethology.* **100,** 50–60.

McNab, B. K. (1980). Energetics and the limits to a temperate distribution in armadillos. *J. Mammal.* **61,** 606–627.

McNab, B. K. (1984). Physiological convergence amongst ant-eating and termite-eating mammal. *J. Zool.* **203,** 485–510.

McNab, B. K. (1985). Energetics, population biology, and distribution of xenarthrans, living and extinct. In *The evolution and ecology of armadillos, sloths, and vermilinguas,* edited by G. G. Montgomery, p. 219–232. Washington, D. C.: Smithsonian Institution Press.

McNab, B. K. (2008). An analysis of the factors that influence the level and scaling of mammalian BMR. *Comp. Biochem. Physiol. A.* **151,** 5–28.

Meyer, A. and Zardoya, R. (2003). Recent advances in the (molecular) phylogeny of vertebrates. *Annu. Rev. Ecol. Evol. Syst.* **34,** 311–338.

Milne, N. and O'Higgins, P. (2012). Scaling of form and function in the xenarthran femur: a 100-fold increase in body mass is mitigated by repositioning of the third trochanter. *Proc. R. Soc. B*. **279,** 3449–3556.

Milne, N., Toledo, N. and Vizcaíno, S. F. (2012). Allometric and group differences in the xenarthran femur. *J. Mammal. Evol.* **19,** 199–208.

Newman, H. H. (1913). The natural history of the nine-banded armadillo of Texas. *Amer. Nat.* **47,** 513-539.

Nowak, R. M. (1999). *Walker's Mammals of the World*, 6th ed. Baltimore: Johns Hopkins University Press.

Nunamaker, D. M., Butterweck, D. M. and Provost, M. T. (1990). Fatigue fractures in thoroughbred racehorses: relationships with age, peak bone strain, and training. *J. Orthop. Res.* **8,** 604–611.

Prudom, A. E. and Klemm, W. R. (1973). Electrographic correlates of sleep behavior in a primitive mammal, the armadillo *Dasypus novemcinctus*. *Physiol. Behav.* **10,** 275–282.

Pujos, F., De Iuliis, G. and Werdelin, L. (2007). A peculiar climbing Megalonychidae from the Pleistocene of Peru and its implications for sloth history. *Zool. J. Linn. Soc.* **149,** 179–235.

Redford, K. H. (1985). Foods habits of armadillos (Xenarthra: Dasypodidae). In G.G. Montgomery, ed. *The evolution and ecology of sloths, armadillos, and vermilinguas.* Washington, DC: Smithsonian Institution Press, p. 429–437.

Reilly, S. M. and White, T. D. (2003). Hypaxial motor patterns and the function of epipubic bones in primitive mammals. *Science* **299,** 400–402.

Reilly, S. M., McElroy, E. J. and White, T. D. (2009). Abdominal muscle function in ventilation and locomotion in new world opossums and basal eutherians: breathing and running with and without epipubic bones. *J. Morphol.* **270,** 1014–1028.

Rhee, H., Horstemeyer, M. F., and Ramsay, A. (2011). A study on the structure and mechanical behavior of the *Dasypus novemcinctus* shell. *Mater. Sci. Eng. C.* **31,** 363–369.

Rubin, C. T. and Lanyon, L. E. (1982). Limb mechanics as a function of speed and gait: a study of functional strains in the radius and tibia of horse and dog. *J. Exp. Biol.* **101,** 187–211.

Salazar-Bravo, J., Vargas, J., Jimenez-Ruiz, A. and Savage, J. M. (2010). A new record of *Attractus boettgeri* (Serpentes: Colubridae), with notes on taxonomy and natural history. Revista Mexicana de Biodiversidad. **81,** 925–929.

Sheffield, K. M. and Blob, R. W. (2011). Loading mechanics of the femur in tiger salamanders (*Ambystoma tigrinum*) during terrestrial locomotion. *J. Exp. Biol*. **214,** 2603–2615.

Sheffield, K. M., Butcher, M. T., Shugart, S. K., Gander, J. C. and Blob, R. W. (2011). Locomotor loading mechanics in the hindlimbs of tegu lizards (*Tupinambis merianae)*: comparative and evolutionary implications. *J. Exp. Biol*. **214,** 2616–2630.

Staller, E. L. (2001). Identifying predators and fates of northern bobwhite nests using miniature video cameras. Master's Thesis, University of Georgia, Athens, Georgia.

Tumlison, R. and Tumlison, C. (1995). Behavior and efficiency of juvenile armadillos (*Dasypus novemcinctus*) foraging on earthworms. *Southwestern Nat*. **40,** 224–225.

Twyver, H. V. and Allison, T. (1974). Sleep in the armadillo *Dasypus novemcinctus* at moderate and low ambient temperatures. *Brain Behav. Evol.* **9,** 107–120.

Vickaryous, M. K. and Hall, B. K. (2006). Osteoderm morphology and development in the nine-banded armadillo, *Dasypus novemcinctus* (Mammalia, Xenarthra, Cingulata). **J. Morphol. 267,** 1273–1283.

Vizcaíno, S. F. and Loughry, W. J. (2008). *The Biology of the Xenarthra.* Gainesville, FL: University Press of Florida.

Vizcaíno, S. F., Milne, N. and Bargo, M. S. (2003). Limb reconstruction of *Eutatus seguini* (Mammalia: Xenarthra: Dasypodidae). Paleobiological implication. *Ameghiniana.* **40,** 89–101.

Walker, W. F. Jr (1971). A structural and functional analysis of walking in the turtle, *Chrysemys picta marginata. J. Morphol.* **134,** 195–214.

Walker, W. F. Jr (1973). Locomotor apparatus of Testudines. In: Gans C, Parsons TS, editors. Biology of the Reptilia: Morphology Vol. 4. London: Academic Press. p. 1–100.

White, T. D. (1990). Gait selection in the brush-tail possum (Trichosurus vulpecula), the northern quoll (Dasyurus hallucatus), and the Virginia opossum (Didelphis virginiana). *J. Mammol.* **71,** 79-84.

Wilson, M. P., Espinoza, N. R., Shah, S. R. and Blob, R. W. (2009). Mechanical properties of the hindlimb bones of bullfrogs and cane toads in bending and torsion. *Anat. Rec.* **292,** 935–944.

Yaksh, T. L. (1967). Observations of behavior and learning in the armadillo (*Dasypus novemcinctus mexicanus*). Master's Thesis, University of Georgia, Athens, Georgia.

Yeni, Y. N. and Fyhrie, D. P. (2003). A rate-dependent microcrack-bridging model that can explain the strain rate dependency of cortical bone apparent yield strength. *J. Biomech.* **36,** 1343-1353.

APPENDIX

INTRODUCTION

The present understanding of the relationship between evolutionary changes in limb bone loading and limb posture in tetrapods remains incomplete. Sources of complexity involve selection of an appropriate limb morphology (i.e., shape and material properties of limb bones) and locomotor strategy to meet the survival needs of a species. Insurance of adequate bone *strength*, *stiffness*, and *toughness* to avoid fracture during routine locomotor behaviors is a critical factor in the evolutionary design of limb bones (Erickson et al., 2002). Strength is defined as the peak load (stress) at which a bone fractures, while stiffness refers to the ability of a bone resist deformation (strain), and toughness is the capability of bone to absorb energy while under load (Currey, 2002). It has been argued that the muscular forces produced during steady locomotion are the most important factors influencing bone morphology (Biewener, 1982). It is also likely that undergoing frequent high magnitude accelerations and decelerations may strongly influence skeletal design (Biewener, 1982, 1983a,b). Rapid changes in velocity during locomotion are major components of the locomotor repertoire of small animals, thus resistance to stress (stress = force/cross-sectional area) is important even when supporting a low body mass on short, crouched limbs.

Resistance to loading is more critical for larger animals that have longer limb bones coupled with upright limb posture. The limb muscles of large, upright animals have a higher effective mechanical advantage to compensate for this size effect (Biewener, 1989, 1990). Importantly, functional locomotor stresses are maintained at similar magnitudes over a range of body sizes, and large animals compensate for the geometric scaling of their skeletons (proportional increases in bone size: isometry) by reducing axial and transverse forces acting on their limb bones (Biewener, 1989). This is achieved by aligning the distal limb bones more closely to the ground reaction force (GRF) vector promoting axial compression, a loading regime in which limb bones are strongest to resist (Currey, 2002). Specifically, limb muscles acting at a high angle to the longitudinal axis of bone can counteract the transverse component of the GRF, which reduces the bending moment (moment = torque), and substantially lowers bone stresses to levels similar to those measured in small animals. However, investigations of locomotor limb bone

loading in extant-terrestrial vertebrates have thus far not indicated a clear evolutionary relationship between bone loading patterns and changes in limb posture. Previous studies (e.g., Blob and Biewener, 1999; Butcher et al., 2008, 2011; Sheffield et al., 2011; Sheffield and Blob, 2011) investigated limb bone loading in non-avian reptiles (and amphibians) and a basal marsupial (opossum) to evaluate both functional and phylogenetic differences across tetrapod taxa. Additional studies of generalized mammals will provide important functional data to better understand diversity in limb bone loading patterns and limb posture, thus improving our ability to trace the evolutionary timing of changes in limb bone design.

Limb bone loading in upright mammals and birds

Classical studies of locomotor bone loading and material properties were performed on the distal limb bones of cursorial-adapted (i.e., running specialized) mammals and birds. In upright mammals and ground birds, three shared features of bone loading are consistently observed during terrestrial locomotion: (i) high bending loads, (ii) low torsional loads, and (iii) low limb bone safety factors. First, their limb bones are primarily loaded in high magnitudes of bending superimposed on axial compression (Biewener, 1990; Biewener and Bertram, 1993). Bending of a bone consists of concomitant tensile (positive) and compressive (negative) forces acting throughout its cross-sectional area about a divisional *neutral axis* (NA), where stress is zero. Bending produces much greater stress than axial compression alone (constant support of the body mass) because the force is concentrated at the bone surface (i.e., unequal loading about the NA) (Bertram and Biewener, 1988). In contrast, when a load is equally distributed over the entire cross-section of a bone, it is a stabile, compressive axial load. Bones are much stronger in compression than in tension (Currey, 1970; Biewener, 1993), and function more efficiently (minimum mass for a given strength) to resist high axial compressive forces (Biewener, 1990). As such, total compressive loads are always higher than tensile loads, and therefore, the peak values presented here for bending load comparisons are peak compressive stresses and strains.

Cursorial mammals such as goats, dogs, horses, and humans experience high bone bending as indicated by *in vivo* recordings of large axial and principal strains (in the unit

microstrain: με). For example, peak compressive strains for dog (Rubin and Lanyon, 1982), goat (Biewener and Taylor, 1986), and horse (Gross et al., 1992) tibiae range between -2000 and -3200 με, whereas peak strains in the human tibia are generally less than -1000 με (Burr et al., 1996). In other studies, the third metacarpus of galloping horses have exceedingly high recorded peak strains ranging from -4000 to -5000 με (Nunamaker et al., 1990; Davies et al., 1993). A corresponding range of peak bending stresses associated with the reported peak strain values of the tibiae are 36.3–46.0 MPa (unit: megapascals) (Rubin and Lanyon, 1982; Biewener et al., 1983; Biewener and Taylor, 1986). Second, off-axis loading (shear or torsion) is either low or absent in the distal limb bones of mammalian species for which data are available (e.g., Lanyon and Bourn, 1979; Rubin and Lanyon, 1982; Biewener et al., 1983, 1988; Biewener, 1993; Main and Biewener, 2004), although torsional loading is observed in femora of chickens (Carrano, 1998) and emus (Main and Biewener, 2007). This is due to a more horizontally oriented femur during the stance phase in these ground birds, allowing torsional loads (recorded as shear strains) to reach levels that double the axial bending strains (Carrano, 1998; Carrano and Biewener, 1999). Interestingly, unusual values of shear strains approaching 2000 με also are observed in the human tibia during uphill sprints (Burr et al., 1996). Perhaps the incline locomotor conditions, the modified hinge joint structure of the human knee (i.e., allows medial and lateral rotation when flexed), and the ability of the ankle joint to move in three planes contribute to this finding. Recordings of *in vivo* bone strains are most often made during level, steady-state locomotion and furthermore, the distal limb joints of quadrupedal cursors are specialized for only sagittal plane motion (Hildebrand, 1960).

Third, limb bone safety factors range from 2–4 in the upright mammals and birds (Alexander, 1981; Biewener, 1993). Safety factors are calculated as the ratio of limb bone failure strain to the peak functional strain a bone may encounter (Bertram and Biewener, 1988). Therefore, the limb bones of upright mammals and birds can experience peak loads up to 4 times greater than the usual loads experienced during steady-state locomotion without failure. As material properties of bone are generally similar across vertebrate taxa regardless of morphology, size, or mode of locomotion (Erickson et al., 2002), high magnitudes of bone bending experienced during functional behaviors become

critical to determining the low margin of safety against bone failure in mammals and birds. That said, it is important to measure bone material properties in a species for which bone loading is directly recorded in order to accurately determine safety factors and their phylogenetic history (Sheffield et al., 2011). Failure stress and strain are measured by *ex vivo* loading of limb bones in bending and torsion using mechanical property testing machines. Briefly, for a bending test, the ends of an excised whole bone are secured in a jig and the bone loaded in three-point bending by an anvil (attached to a load cell) pressing into the mid-shaft (at a constant loading rate) until the bone fractures. A torsion test involves casting the ends of a whole bone into mounting brackets and the bone is twisted (also at a constant loading rate) until the bone fails through torsion. Failure of a bone occurs when stress exceeds the strength of the tissue, but morphological features of bone act to prevent this from occurring. Limb bones retain an inherent longitudinal curvature (Bertram and Biewener, 1988) over a large range of body size (Biewener, 1983b). This attribute provides a mechanism for loading predictability, and is argued to play an important role in the safety factors of limb bones (Biewener, 1993). Currey (2002) supports this argument suggesting that despite reducing ultimate strength, bone curvatures act as internal biomechanical load receptors that provide a warning to an animal when bones are nearing their stress/strain limits. Animals can use this mechanical sensory feedback to change their locomotor behaviors (e.g., reduce running speed) to reduce the levels of bone loading.

Limb bone loading in sprawling non-avian reptiles and amphibians

Non-avian reptiles and amphibians exhibit a much different limb posture than upright mammals and birds, along with notable differences observed in their limb bone loading magnitudes and regimes. Previous studies evaluated limb bone loading and material properties in alligators and iguanas (Blob and Biewener, 1999; Blob and Biewener, 2001), turtles (Butcher and Blob, 2008; Butcher et al., 2008), tegu lizards (Sheffield et al., 2011), salamanders (Sheffield and Blob, 2011) and bullfrogs and cane toads (Wilson et al., 2009). All of these animal groups have in common a sprawling limb posture in which their proximal limb bones (e.g., femur) are oriented lateral to the body (i.e., within the transverse plane) (Walker, 1971, 1973; Gatesy, 1991) versus the parasagittal limb

posture seen in upright mammals and birds where their limbs are aligned vertically beneath the body (Jenkins, 1971). Accordingly, limb bone loading patterns for sprawling animals during terrestrial locomotion differ from upright mammals and birds by the following three observations: moderate bending loads, high torsional loads, and high limb bone safety factors (Blob and Biewener, 2001; Butcher and Blob, 2008; Sheffield et al., 2011). First, mean peak compressive strains of the femur and tibia range from -300 to -1100 με (Blob and Biewener, 1999; Butcher et al., 2008; Sheffield et al., 2011), which translate into peak compressive stress values of approximately -13 to -37 MPa (Blob and Biewener, 2001; Butcher and Blob, 2008; Sheffield and Blob, 2011). Thus, extremely high magnitudes of bending in sprawling species approach only the low end of the bending load range in upright mammals. Second, substantial recorded shear strains relate to the high torsional loads of non-avian reptiles. For example, river cooter turtles (*Pseudemys concinna*) have high shear strains of 1500–3500 με in their femur during walking (Aiello et al., *in press*), marking the highest levels of limb bone torsion recorded in any animal during terrestrial locomotion. Moderate-to-high levels of torsion occur because of the high angle of the laterally directed femur relative to the position of the resultant GRF vector causing either internal or external rotation of the bone throughout a step (Butcher and Blob, 2008). Axial rotation of the femur has to be resisted by high force of hindlimb muscles acting to counteract the rotation. The combination of these forces is responsible for the high magnitudes of shear strains recorded on the mid-shaft surfaces of the femur (Sheffield et al., 2011).

Third, a major feature of non-avian reptile and amphibian locomotion, and noteworthy difference of this group compared to upright mammals and birds, are high safety factors in bending ranging from 6.3–13.9 (Blob and Biewener, 1999; Blob and Biewener, 2001; Butcher and Blob, 2008; Butcher et al., 2008; Sheffield and Blob, 2011). Comparative locomotor (walking) and bone material properties data from turtles and salamanders indicate lower limb loads, higher bone strength, or a combination of these parameters to yield high safety factors (Butcher and Blob, 2008; Butcher et al., 2008; Wilson et al., 2009; Sheffield and Blob, 2011). The findings of these inclusive studies challenge the findings of Erickson et al. (2002) and suggest that reptilian limb bones are ‘over-designed’. Questions surrounding this hypothesis are subject to debate. Elevated safety

factors may have been retained ancestral trait that was not costly enough to be selected against (Blob and Biewener, 1999; Butcher and Blob, 2008). Some of the most convincing evidence in support of this argument is demonstrated by walking tiger salamanders where the safety factor of the femur is 10.5 in bending (Sheffield and Blob, 2011). Because of their classification as an out-group to amniotes (Gao and Shubin, 2001), retention of high limb bone safety factors in this lineage is likely ancestral rather than a result of having additional functional requirements (e.g., higher bone strength) beyond those of mammals and birds (Butcher and Blob, 2008; Butcher et al., 2008). Moreover, convergent evolution among cursorial mammals and birds with lower limb bone safety factors may have occurred instead of these traits (e.g., high bone strength and safety factors) being inherited from a common ancestor of terrestrial tetrapods (Butcher et al., 2008). Other factors such as variability in femoral stresses, lower rates of microdamage, and bone remodeling (compared with mammals) could have led to higher safety factors in non-avian reptiles and amphibians (Blob and Biewener, 1999; Blob and Biewener, 2001). In either circumstance, elevated limb bone safety factors are advantageous because of the decreased likelihood of failure under normal or abnormal locomotor loading conditions (Carter et al., 1981).

Limb bone loading in crouched mammals

The differences in bone loading magnitudes and regimes between upright mammals and sprawling reptiles suggest that limb bone loading and design are directly related to limb posture (Butcher and Blob, 2008; Sheffield et al., 2011). This relationship is supported by a recent evaluation of femoral loading in the hindlimb of the terrestrial Virginia opossum (*Didelphis virginiana*) (Butcher et al. 2011; Gosnell et al., 2011). This generalist marsupial (metatherian) belongs to a clade phylogenetically between upright mammals and sprawling reptiles (Meyer and Zardoya, 2003), and has a crouched limb posture unique from those lineages. Many small mammals (and basal lineages of mammals) exhibit a crouched limb posture where the joints are more flexed and limbs move with near-parasagittal kinematics (Jenkins, 1971). Similar to both mammals and non-avian reptiles (and amphibians) for which bone loading data have been collected, the loading regime that the opossum femora encounter during terrestrial locomotion is a combination

of axial compression, bending, and torsion (Butcher et al., 2011). As previously indicated, bone bending is typical of all terrestrial mammals; however, the direction of bending is mediolateral in the opossum femur (Butcher et al., 2011), and thus is atypical to the pattern of anteroposterior bending observed in the limb bones of upright mammals (Rubin and Lanyon, 1982; Biewener et al., 1983, 1988; Biewener and Taylor, 1986). Mean peak compressive strains in opossum femora approach -2300 με (Butcher et al., 2011) and peak compressive stresses are approximately -35 MPa (Gosnell et al., 2011). Interestingly, these magnitudes of loading (i.e., high compressive loads in bending) are near the low end values of upright mammals and birds, but approximate the high end values of non-avian reptiles and amphibians.

It is also interesting to find that opossum femora undergo appreciable torsion throughout a running step with mean peak shear strains of nearly 2000 με (Butcher et al., 2011). This magnitude of torsional loading is substantially higher than that measured in limb bones of any cursorial mammal, and yet similar to levels found in the femora of alligators and lizards (Blob and Biewener, 1999; Sheffield et al., 2011). The levels of shear strain in the opossum femur are also consistent with loading patterns in rats, which share a crouched limb posture, and have femoral shear strains 3-fold higher than axial strains (Keller and Spengler, 1989). Moreover, shear strains of both opossums and rats are comparable to those of chickens (Carrano, 1998) and emus (Main and Biewener, 2007) that experience shear strains slightly greater than 2000 με in their femora. Lastly, the safety factor in bending for opossum femora is 8.1, and this value may be due to magnitudes of bending that were 2-fold lower compared to upright mammalian species (Gosnell et al., 2011). Because of their surprisingly high magnitudes of shear strains, the safety factor in torsion is comparable to that of upright mammals (Butcher et al., 2011) which have relatively low resistance to failure by torsional loads (Currey, 1984, 2002). Collectively, functional bone data from the opossum indicate loading patterns and properties that are intermediate to upright mammals and sprawling reptiles. To better understand if loading patterns and bone mechanical properties of crouched posture animals in general, are intermediate to those of upright mammals and sprawling reptiles, requires functional loading data from a greater diversity of generalist mammals that use non-parasagittal limb kinematics during terrestrial locomotion. Table 1 summarizes all

available data on comparative values of peak bending and torsional strains, and safety factors across vertebrate taxa.

Biology, behavior, and morphology of armadillos

Armadillos (Family: Dasypodidae) are a branch of the order Cingulata (Superorder: Xenarthra), which evolved approximately 65 million years ago (Delsuc et al., 2012), making armadillos one of the earliest extant placental (eutherian) mammals. Their closest relatives are from the other branch of Cingulata known as Pilosa, and consist of anteaters and sloths (Delsuc et al., 2012). Dasypodinae, a subfamily, evolved nearly 40 million years ago and contains the closest relatives to the nine-banded armadillo *(Dasypus novemcinctus*) (Delsuc and Douzery, 2008). Nine-banded armadillos evolved 11 million years ago (Delsuc et al., 2012) in present day South America, and since have spread north to inhabit the southern regions of the United States as the northern end of their range (McDonough and Loughry, 2013). Nine-banded armadillos exhibit a generalized body plan along with some unique features, including fossorial specialized (i.e., digging) forelimbs and a distinctive carapace composed of rings or bands of dermal bone (see below). The hindlimbs of armadillos have features typical of terrestrial locomotor habits (Fariña and Vizcaíno, 1997; Vizcaíno and Milne, 2002). Thus, *D. novemcinctus* is a model species for evaluating femoral loading patterns that might approximate those of ancestral mammals prior to them evolving running specializations.

Armadillos are solitary animals (Loughry and McDonough, 2013) spending most of their total time budget in burrows that they either dig or come to occupy. *D. novemcinctus* is a particularly resourceful species that typically refurbishes old burrows to save energy. They are capable of digging to depths of 0.5 m in a few hours by excavating with the forelimbs and removing dirt from the burrow with the hindlimbs (Loughry and McDonough, 2013). This depth is enough to hide their bodies, which range in length from 61.5–80 cm, and includes a tail 24.5–37 cm in length (McBee and Baker, 1982). Moreover, their body mass is sexually dimorphic with females ranging from 3.6–6.0 kg and males 5.5–7.7 kg (McBee and Baker, 1982). The need to conserve energy is critically important to the biology of armadillos. For this reason, they are frequently active at night (Kalmbach, 1943) when temperatures are cooler. In general, armadillos

display low levels of activity, and have poor thermoregulatory abilities and low metabolic rates, features that are common across all xenarthrans (McNab, 1984, 1985, 2008; Clarke et al., 2010). In fact, the metabolic rates of armadillos are among the lowest reported for any placental mammal (McNab, 1980). Moreover, studies of their circadian rhythms indicate they sleep 16–18 hours a day (Prudom and Klemm, 1973; Twyver and Allison, 1974). Most of their active time (~80%) is spent foraging for insects, where a walking gait is commonly used to move between forage sites (Ancona and Loughry 2009). Armadillos (genus *Dasypus*) are considered to be insectivore generalists (Redford, 1985) with a diet primarily composed of beetles, ants, and termites (Loughry and McDonough, 2013). *D. novemcinctus* is known to consume numerous other insects including wasp and butterfly larvae, grasshoppers, and flies (Kalmbach, 1943), along with earthworms (Tumlison and Tumlison, 1995) and vertebrates such as frogs, lizards, and snakes (Salazar-Bravo et al., 2010). Dirt and eggs of ground-nesting birds (e.g., northern bobwhite eggs) (Bushnell, 1952; Breece and Causey, 1973; Staller, 2001) are also important components of the diet of *D. novemcinctus*.

Nine-banded armadillos exhibit a rear plantigrade foot posture (calcaneus is in contact with the ground) and tend to support most of their body mass on their hindlimbs (Frechkop, 1949). Thus, their limb bone proportions and mass scale (i.e., body size relation) more like generalized walking mammals than specialized diggers (Fariña and Vizcaíno, 1997). In addition to lateral sequence walking, *D. novemcinctus* also use a walk-run and a trot to locomote at higher speeds (Loughry and McDonough 2013). Each of these gaits is defined as symmetrical, where footfalls are evenly spaced in time, and allow the animal to achieve moderately fast running speeds (Hildebrand, 1985). Trotting is only seen during avoidance of dangers prompting a quick escape, while a walk or walk-run is observed as typical locomotion (Loughry and McDonough, 2013). Perhaps most familiar is their startle response involving vertical or forward jumps to escape a threatening situation. During times of potential danger and during the mating season, armadillos also display an interesting vigilance behavior. It involves rearing up on hindlimbs for bipedal sniffing using the tail for balance. This posture allows them to better detect the odors of predators (McDonough and Loughry 1995) and or places male armadillos in a more strategic position for monitoring the movements of potential female

mating partners. The time allocated for vigilance is observed to be less than 5% of their active time budget and this may be due in large part to limited predation on these animals (Loughry and McDonough, 2013). Lastly, nine-banded armadillos can also engage in chases that turn to acts of aggression where they kick other armadillos with the hindlimbs and scratch with the sharp foreclaws. Aggressive armadillos may also jump, and flip in the air, to dodge or deliver wounding blows to other animals (Yaksh 1967; Denson 1979; McDonough 1994).

Functional Morphology

The most distinctive external characteristic of armadillos is their carapace. The carapace consists of three sections including an anterior scapular shield, carapace bands, and pelvic shield. Small calcified structures form in the dermis of the skin called osteoderms, or scutes (Vickaryous and Hall, 2006), and articulate to compose this protective layer of tissue (Chen et al, 2011; Rhee, Horstemeyer, and Ramsay, 2011). The limbs and tail are also reinforced with scutes, and the tail armor is fused with the caudal vertebrae (Loughry and McDonough, 2013). The carapace is a relatively tough structure (Chen et al., 2011; Rhee et al., 2011) serving to protect the armadillo from physical damage from both predators and escapes through thick, thorny vegetation (Newman, 1913). In the event of a failed escape to their burrow, armadillos will also flatten their bodies to become less conspicuous to predators (Loughry and McDonough, 2013).

Armadillos are xenarthrans, a name derived from the xenarthrous vertebrae that have supplemental intervertebral articulations, known as xenarthrae (Gaudin and Biewener, 1992). Xenarthrae serve to stiffen the vertebral column and may also serve to transmit large forces generated by forelimbs during digging to the pelvis and hindlimbs (Jenkins, 1971). Specifically, torsion tests of individual vertebral displacements show that rotation is absent in posterior thoracic and lumbar vertebrae in *D. novemcinctus,* and their overall vertebral column is stiff in dorsal and lateral bending (Gaudin and Biewener, 1992). The presence of xenarthrae and the stiff structure of the vertebral column representing adaptations for digging mechanics may provide an explanation for the inability of armadillos to gallop (asymmetrical fast-running gait). Interestingly, opossums share a similar inability to gallop, although their body axis is made stiff by the actions of hypaxial and epaxial muscles (e.g., long pectineus muscles) inserting on epipubic bones

that arise from the femur (Reilly and White, 2003; Reilly et al., 2009), instead of the presence of vertebral xenarthrae.

Observations of the femora of xenarthrans also point to bony modifications. The bony landmarks of the femur that show varying degrees of specialization are the femoral head, greater trochanter, and distal articular condyles (Fig. 1). Armadillos have a superiorly and anteriorly positioned greater trochanter, a larger medial condyle compared to the lateral condyle, and the shaft of their femur shows a pronounced medial concavity (Milne et al., 2012). A third trochanter (T3) is also present along the lateral aspect of the femoral shaft and this feature is unique to xenarthrans (McDonald and Iuliis, 2008; Milne et al., 2012). In armadillos, the T3 is located just proximal to the mid-shaft (see Fig. 1). Increases in body size among similar species shifts the T3 location more distally along the femoral shaft (Vizcaíno and Milne, 2002; Milne et al., 2012). Whereas the *m. gluteus medialis* and *m. gluteus profundus* (hip abductor/flexors) insert on the greater trochanter, the third trochanter receives insertions from the *m. gluteus superficialis* (analogous to gluteus maximus) and *m. tensor fasciae latae* (Vizcaíno et al., 2003). The latter two muscles generally act to extend and abduct the hip joint, respectively (Argot, 2002; Milne and O'Higgins, 2012). However, because the greater trochanter is positioned superior to the head of the femur in the armadillo (Fig. 1), the muscle moment arm of the gluteal muscles is reduced and thus they are relatively weak hip abductors (Pujos et al., 2007). Moreover, the medial origin of the *m. tensor fasciae latae* on the iliac crest indicates this muscle would cause medial rotation of the femur to stabilize the hip joint in coordination with the actions of the gluteus medialis and profundus (Milne and O'Higgins, 2012). Therefore, considering the large mass of the *m. gluteus superficialis* and hamstring musculature (e.g., *m. biceps femoris*), and the long muscle moment arm of the gluteus superficialis by its insertion on the T3, armadillo hindlimbs have a mechanical arrangement that promotes powerful hip extension by retraction of the femur during locomotion (Milne et al., 2012).

A recent study modeled loading of the armadillo femur (species: *Chaetophractus villosus*) by finite element analysis (FEA). This method involves digitizing three-dimensional coordinates of a bone for use in a geometric morphometric analysis. In principle, the model attempts to simulate bone loading that occurs during weight bearing

and locomotion. Simulation results during loading show mediolateral bending and tensile strains that differ in magnitude superior and inferior to the third trochanter along the lateral aspect of the femur (Milne and O'Higgins, 2012). Mediolateral bending of the femur indicates that bone bending is taking place in a coronal (frontal) plane through the femur about an anteroposterior oriented NA. Despite the inability of the model to predict off-axis loading in torsion, their analyses did consider differences in bending magnitudes related to body size and position of the T3 (Milne and O'Higgins, 2012). The results further suggest bending strains are reduced with a more distally positioned T3 that occurs in species with larger body size (Vizcaíno and Milne, 2002; Milne et al., 2012). This may have important implications for femoral loading in *D. novemcinctus* which exceeds the body mass of the model species *C. villosus* (0.84 kg: Nowak, 1999) by approximately 5 kg. Further analyses must be conducted through *in vivo* experimentation to confirm these modeling predictions and also evaluate torsional loading in armadillo femora. Currently, there are no functional data (bone or muscle) available for any species of armadillo during locomotion.

Objectives and Hypotheses

In summary, studies of upright mammals and birds find three common features in the limb bone loading of these taxa during terrestrial locomotion. First, limb bones are typically loaded by high magnitudes of bending. Second, torsional loading is low, though high torsion has been indicated in the femora of bipedal birds. Third, limb bones of mammals and birds are only strong enough to resist loads 2–4 times greater than usual before failure (safety factor). However, studies of non-avian reptiles (e.g., lizards, alligators, and turtles) and amphibians consistently find patterns of bone loading and design different from those typical in mammals or birds: (1) their limb bones experience moderate bending loads, (2) their limb bones experience substantial torsional loads, and (3) their limb bones have higher safety factors, resulting from both lower magnitude bone bending and higher resistance to failure than found in mammals and birds. Interestingly, opossums and rats, which walk on crouched limbs, have appreciable torsion in their femur while the bone is undergoing unusual mediolateral bending. In general, the loading magnitudes and limb bone safety factors of the opossum are intermediate to upright

mammals and sprawling reptiles. These recent findings from primitive lineages of reptiles and basal mammals suggest the potential for greater diversity in limb bone loading patterns and design than previous mammalian and avian studies had indicated, but explanations for the differences in bone loading among these lineages are not resolved.

Could the loading patterns seen in opossum limb bones, and possibly in other generalist mammals, be retentions of ancestral traits that were not too costly to have been selected against, and from which running mammals and birds have independently diverged? To address such a question and evaluate the evolutionary history of limb bone loading and design patterns, data from a broader range of vertebrate lineages are required. Studies of *D. novemcinctus* provide a possibility for unique insights in this context. First, armadillos exhibit a generalized body plan and a crouched limb posture, in contrast to the running specialists examined previously (e.g., dogs, goats, horses, etc.). Second, armadillos represent one of the most primitive extant mammalian groups. Therefore, *D. novemcinctus* is an excellent model for evaluating limb bone loading conditions that might be close (in evolutionary timing) to those of the ancestor of mammals prior to evolving running specializations.

The objective of this study is to record in vivo strains in the femur during steady-state locomotion to test the hypothesis that the magnitudes and patterns of bone loading experienced by armadillos is an ancestral trait of early mammals. Based on the inherent medial curvature of the femur, the location of the third trochanter near mid-shaft, and the results of modeling analyses of femoral loading, it is predicted that the femur will experience moderate levels of mediolateral bending during running. The large medial condyle suggests it may bear more load and increase stress on the medial cortex of the femoral shaft, placing it into compression and the lateral cortex in tension. This loading pattern would match that of opossum femora (Butcher et al., 2011), although strain magnitudes along the lateral cortex are likely to differ superiorly and inferiorly to the third trochanter in *D. novemcinctus*. In addition to bending, torsional loads are expected to be appreciable. This is predicted because of the use of non-parasagittal limb kinematics that should produce shear strains in the femur similar to opossums. Finally, limb bone safety factors (bending and torsion) are predicted to be intermediate to those of sprawling reptiles and upright mammals. This finding also would be similar to opossums, and

support the hypothesis that the femoral loading regime and design observed in these basal mammals that maintain a crouched limb posture is ancestral.

Table 1. Morphometric data for all experimental animals.

Animal	Sex	Limb	Body mass (kg)	Femur length (cm)	Proximal femur length (cm)	Transverse femur width (cm)	Femoral robusticity index (FRI)	Hip moment index (HMI)
a01	M	L	3.75	9.55	4.93	1.32	0.14	0.52
*a02**	F	L	3.80	9.38	4.77	1.17	0.13	0.51
a03	M	L	3.45	9.02	4.54	1.17	0.13	0.50
a04	F	L	3.60	9.11	4.75	1.17	0.13	0.52
			3.65±0.2	**9.3±0.2**	**4.7±0.2**	**1.2±0.1**	**0.13±0.01**	**0.51±0.01**

*animal lost after surgery

Values in bold are mean±s.d. (standard deviation)

Measurements and functional Indices are adapted from Vizcaíno and Milne (2002). Femur length (FL): maximum femur length; proximal femur length (PFL): length from the proximal point on femoral head to the tip of the third trochanter (T3); Transverse femur width (TFW): mediolateral width of the femur just distal to the T3; Femoral robusticity index (FRI): ratio of TFW to FL; Hip moment index (HMI): ratio of PFL to FL.

Table 2. Peak axial (ε_{axial}), principal tensile (ε_t), principal compressive (ε_c), angle phi (ϕ_t), and shear strains recorded from the femur of *D. novemcinctus*.

Gauge location	ε_{axial} (με)	ε_t (με)	ε_c (με)	ϕ_t (deg)	Shear (με)
'Anterolateral'	1226±560.2 (36, 1)				
'Anterior'	196.1±46.8 (61,1)	202.4±49.9 (61, 1)	-799.3±166.7 (61, 1)	14.8±6.5 (61, 1)	162.5±56.1 (61, 1)
'Anteromedial'	-412.9±236.3 (127, 3)	404.6±151.9 (30, 1)	-737.7±239.1 (30, 1)	16.8±6.1 (30, 1)	463.5±173.3 (30, 1)
'Medial'	-168.9±138.0 (127, 3)				
		269.1±135.0	**-779.0±216.9**	**15.5±6.4**	**261.8±179.0**

Data are mean±s.d.
Values in bold are pooled means across all individuals.
Angles of principle tensile strains to the long axis of the bone (ϕ_t).
In parentheses are the number of steps analyzed and the number of individuals tested, respectively.
Positive angles for ϕ_t indicate inward (medial) rotation for all gauge locations.

Table 3. Mechanical properties, estimated actual peak strains and safety factors for the femur of *D. novemcinctus* loaded in three-point bending.

Mechanical properties				**Mean peak strains**		**Safety factors**
Yield strain tensile (με)	Yield strain compressive (με)	Proportional increases in strain		Calculated tensile (με)	Calculated compressive (με)	Femur bending range
3716.7±419.1 (4)	-4168.4±2802.6 (4)	3.99 t	1.04 c	1614.2	-831.3	2.3–5.0

Mechanical property values are mean±s.d.; number of bones tested is in parentheses.
t, tensile; c, compressive
Peak strain estimates were calculated based on planar strain distributions; these provided a quantitative measure of proportional increases in principal strains (Table 2) used to determine estimated peak strains. Safety factor calculations are described in the text.

Figure 1. Anatomical drawing of the right hindlimb of *D. novemcinctus*. Rosette (ROS) and single element (SE) gauges were implanted about the mid-shaft of the femur. SE gauges (x2) were attached to either the 'anterolateral' (shown), 'anteromedial' (proximal, shadowed gauge), or 'medial' (distal, shadowed gauge) aspects of the femur, while the ROS (x1) was attached to either the 'anterior' or 'anteromedial' locations.

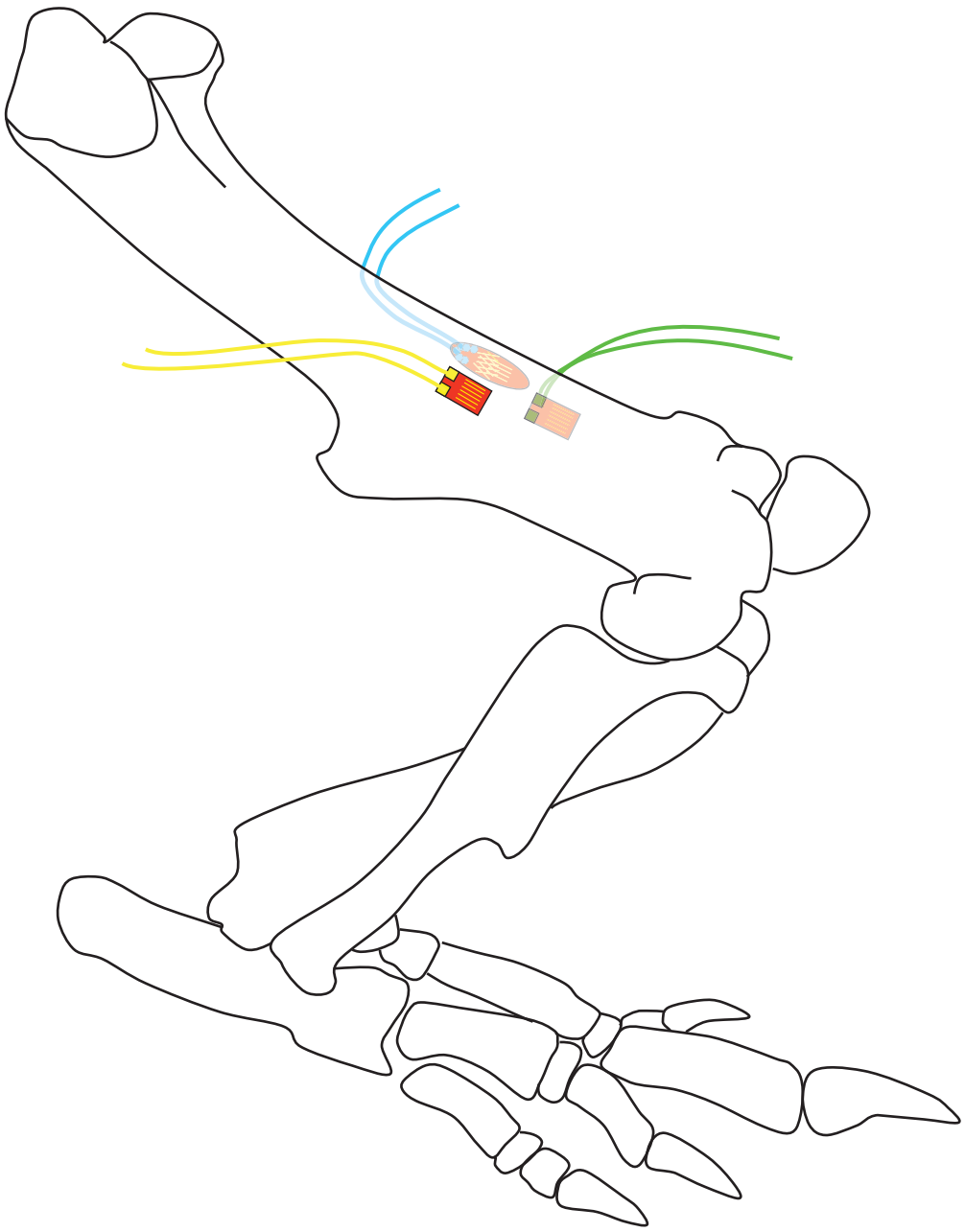

Figure 2. Representative strain recordings from three gauge locations on the femur of armadillo a04 during treadmill locomotion (at maximum speed: 0.55 m s^{-1}). Principal strains, angle of principal tensile strains from the femoral long axis (ϕ_t) and shear strains from ROS gauge recordings on the anterior surface are shown, as well as axial strains from 'anterior,' 'anteromedial,' and 'medial' locations. Strain scales differ among panels to facilitate presentation. Dark gray shading marks the stance phase (contact) for a single step at all gauge locations; light gray shading marks the swing phase of a stride. Top trace: ε_t and ε_c denote tensile (black line) and compressive (red line) principal strains, respectively.

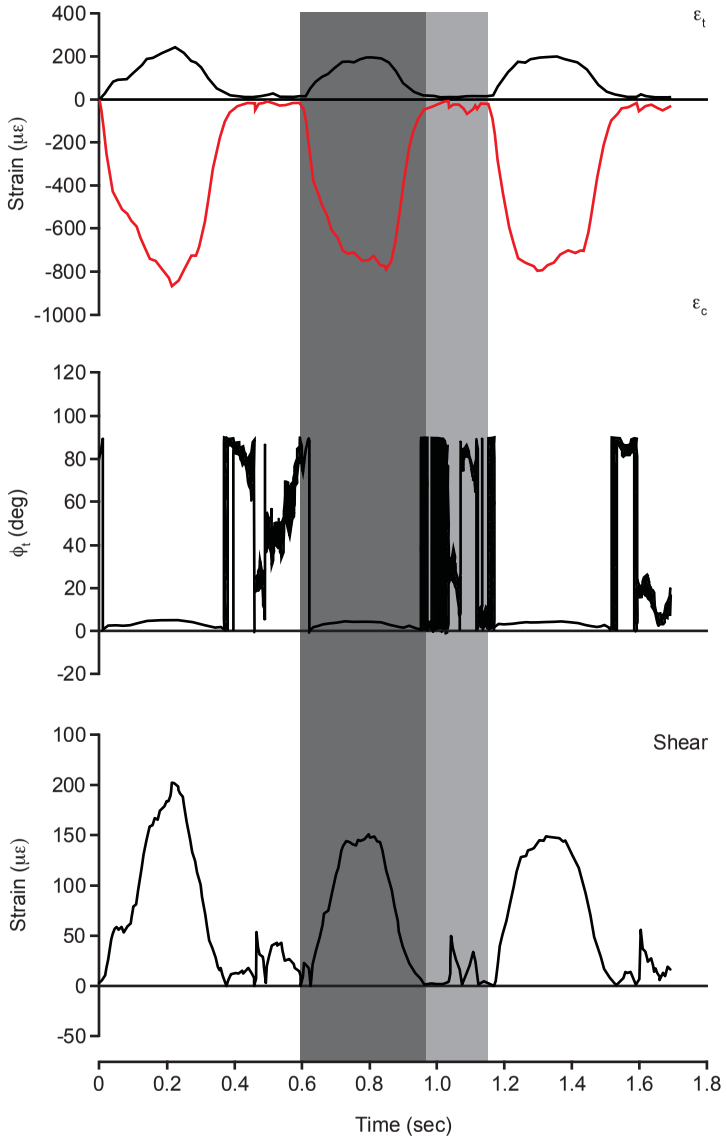
Strain (με)
ε_t
ε_c
ϕ_t (deg)
Shear
Strain (με)
Time (sec)

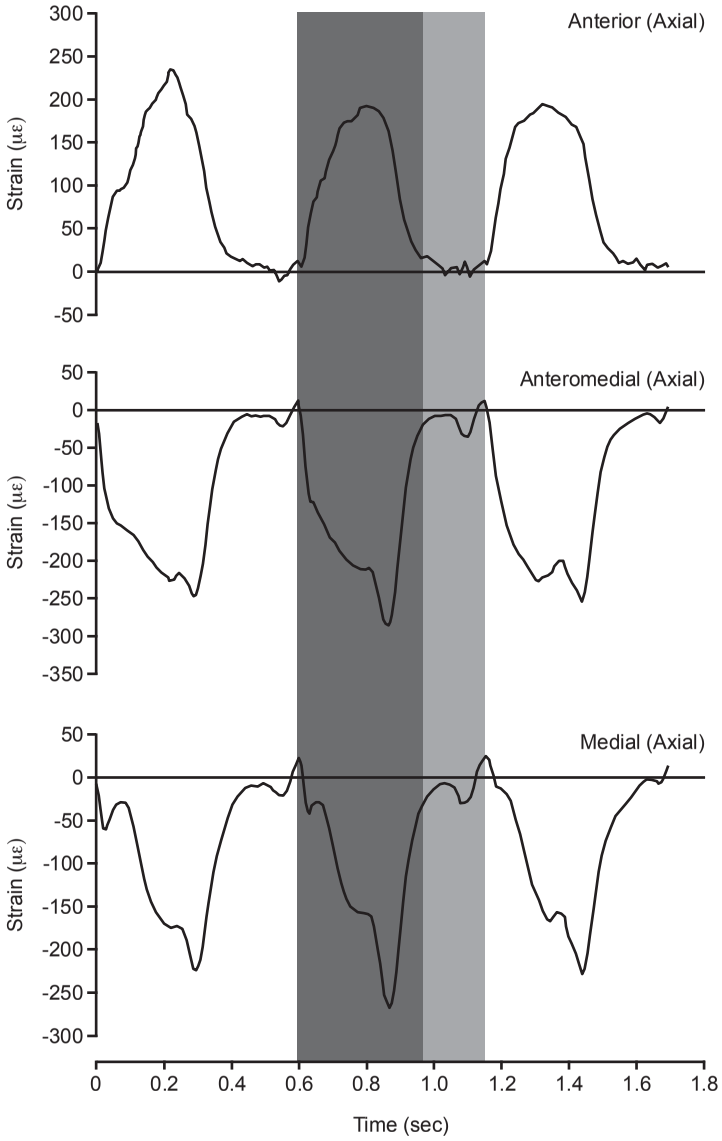
Anterior (Axial)
Strain (με)
Anteromedial (Axial)
Strain (με)
Medial (Axial)
Strain (με)
Time (sec)

Figure 3. Neutral axis orientation in the armadillo femur during treadmill locomotion. (**A**) Shifts in the orientation of the neutral axis (NA) of femoral bending at five time increments (% of contact) through the duration of the step for two individual armadillos. Each data point represents the angle of the NA to the anatomical mediolateral (ML) axis of the femur averaged over n=8–10 steps. The direction of bending indicated by these angular values is indicated by the scale to the right of the panel, with respect to the anatomical axes of the bone as described in the text, not in an absolute frame reference. AP, bending about an NA running from the anatomical medial to lateral cortex; ML, bending about an NA running from the anatomical anterior to posterior cortex. (**B**) Schematic cross-sections of the femur illustrating NA orientation and shift. Strain gauge locations are indicated by the black bars around the cortex of the cross-section. Solid red lines show the NA with an orientation of 100º (top) or 130º (bottom) relative to the anatomical ML axis; vertical dashed lines indicate the anatomical AP axis.

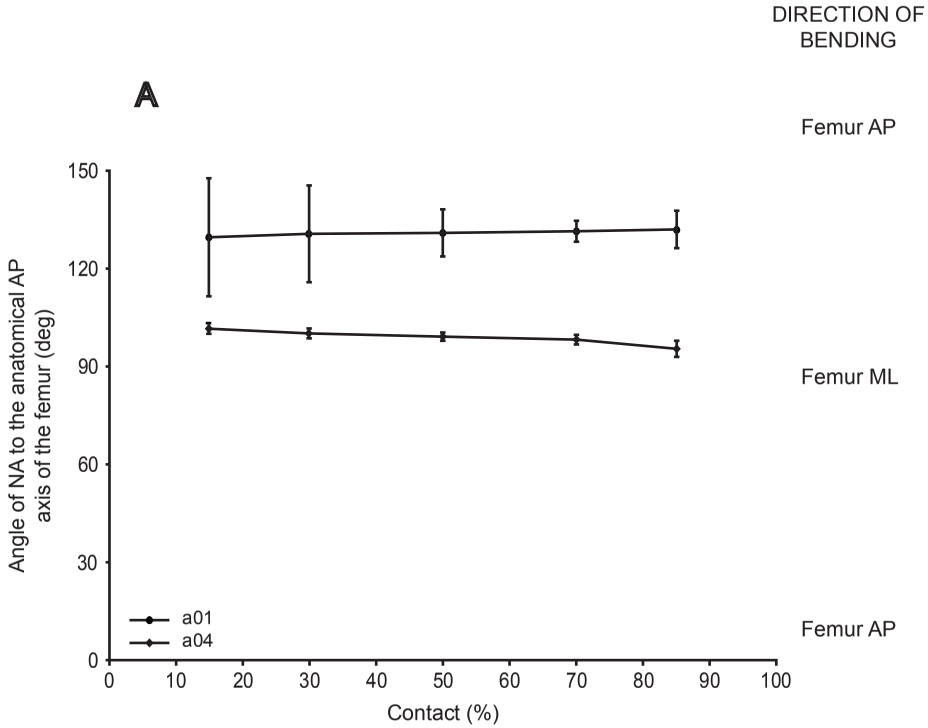
A
DIRECTION OF BENDING
Femur AP
Femur ML
Femur AP
Angle of NA to the anatomical AP axis of the femur (deg)
150
120
90
60
30
0
0
10
20
30
40
50
60
70
80
90
100
Contact (%)
a01
a04

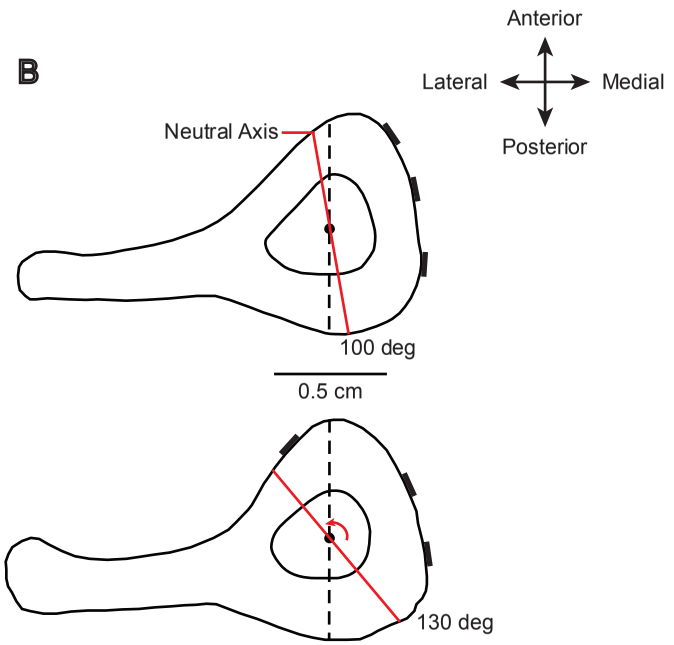
B
Anterior
Lateral
Medial
Posterior
Neutral Axis
100 deg
0.5 cm
130 deg

Figure 4. Graphical comparisons of cross-sectional planar strain analyses in the femur. Femoral strain distributions were calculated for five time increments (% of contact) during representative steps for armadillos a01 (left) and a04 (right). Time increments correspond to those plotted in Fig. 3A. The centroid of each section is indicated by the black dot. Thin lines indicate contours of strain magnitude, each representing 500 με. Dashed lines approximate the ovoid cross-section of the femur. Calculated peak strains for these steps are labeled on the cross-sections at either 70% (a01) or 50% (a04). Compressive strains are shaded gray. The NA of bending (strain=0 με) is indicated by the red line (strain contour) separating compressive and tensile strains. Strain gauge locations are indicated by the black bars around the cortex of each cross-section. Anatomical directions are the same as illustrated in Fig. 3B.

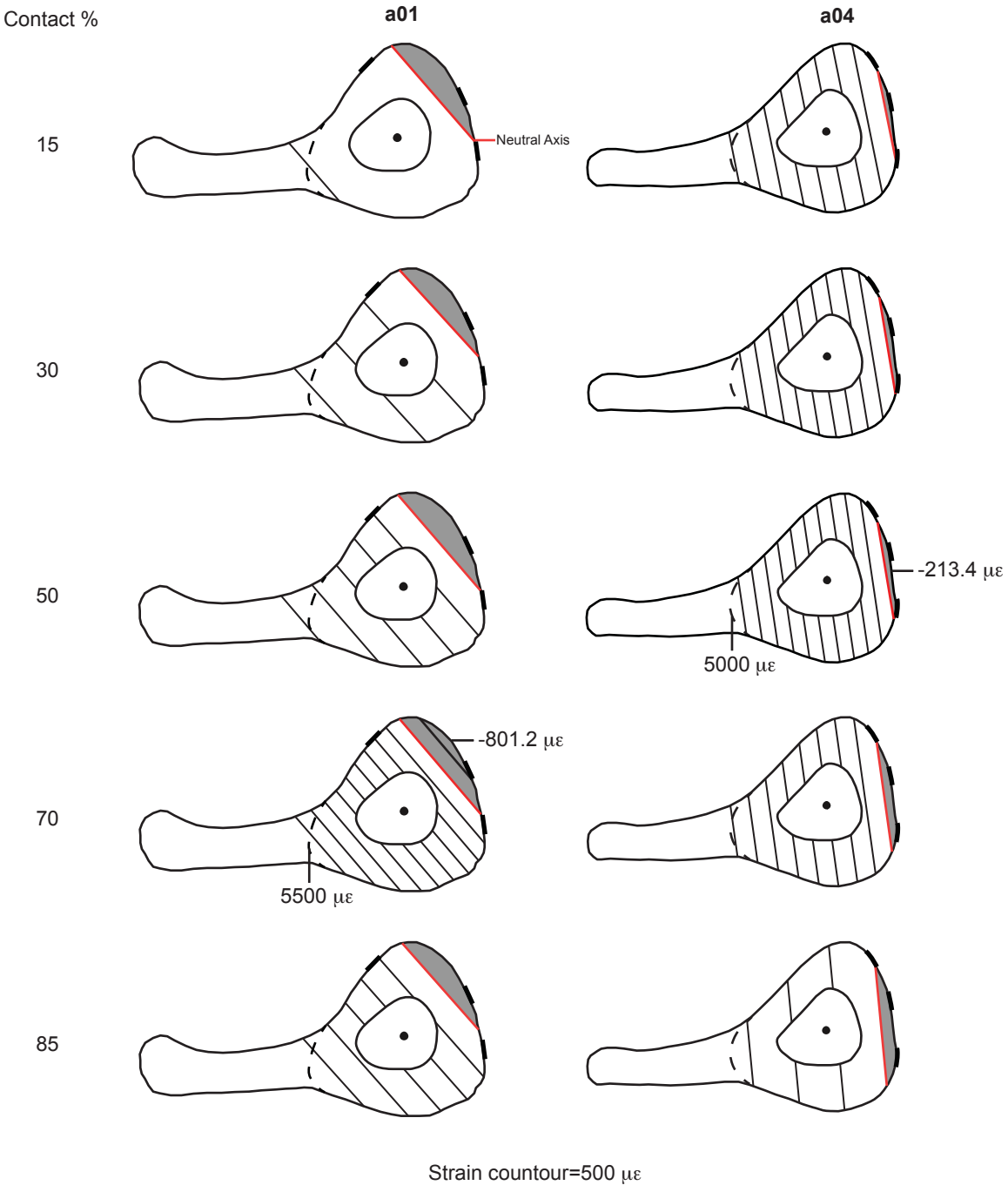
Contact %
a01
a04
15
30
50
70
85
Neutral Axis
-213.4 με
5000 με
-801.2 με
5500 με
Strain countour=500 με

Figure 5. Mechanical properties testing in bending for the armadillo femur. (**A**) load-deformation curve in three-point bending (bending moment vs. recorded strain) and (**B**) representative planar strain calculation of peak yield strains. Bending moments were calculated as load multiplied by the bending moment arm, which equaled one half the gauge length (26 mm) (i.e., distance between the support anvils). Strain contours equal 1000 με.

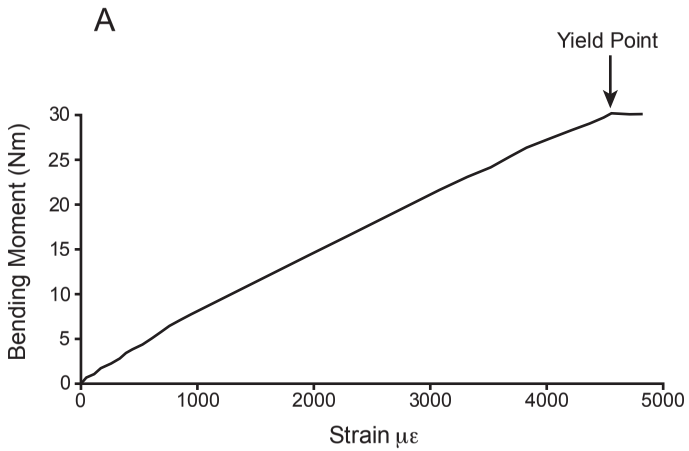
A
Yield Point
Bending Moment (Nm)
30
25
20
15
10
5
0
0
1000
2000
3000
4000
5000
Strain με

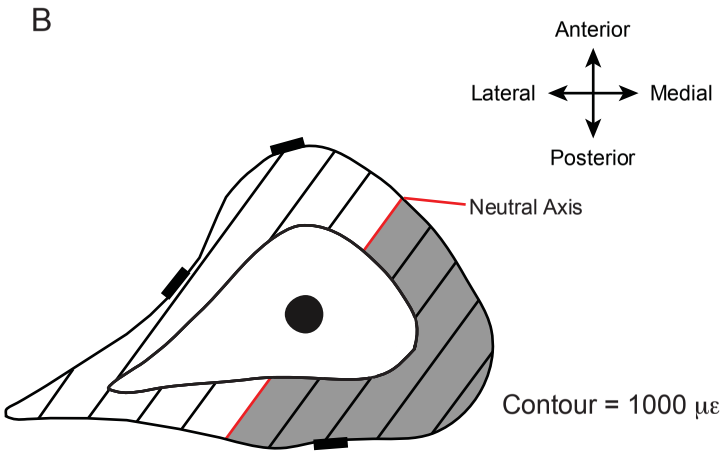
B
Anterior
Lateral
Medial
Posterior
Neutral Axis
Contour = 1000 με

CLEMSON UNIVERSITY

M E M O R A N D U M

To: Dr. Rick Blob

From: Peter Skewes, Ph.D., Chair [redacted]
Institutional Animal Care and Use Committee

OFFICE OF
RESEARCH COMPLIANCE

Clemson University
321 Calhoun Drive
Room 223 Brackett
Hall
Clemson, SC
29634-5704

P 864-656-1525
F 864-656-4475

Subject: Animal Use Protocol Number 2013-030
Titled: Limb Bone Loading in Armadillos

Date: June 12, 2013

Animal Use Protocol Number 2013-030 has been approved by Designated Member Review of the Institutional Animal Care and Use Committee. Approval is for three years from June 12, 2013 and will close on June 12, 2016.

An animal usage and progress report is required and is due by:
June 12, 2014
June 12, 2015

A final animal usage and progress report is due by:
June 12, 2016

Please advise the Institutional Animal Care and Use Committee regarding any proposed changes in personnel, animal procedures, animal models or animal numbers. Any changes must be pre-approved by the Institutional Animal Care and Use Committee.

This institution has an Animal Welfare Assurance on file with the Office of Laboratory Animal Welfare. The Assurance number is A3737-01. Please feel free to contact the IACUC if we may provide assistance as you conduct your research.

CC: GSRC
V. Young